Local Holographic Superconductors and Hovering Black Holes

by

Atakan Hilmi Fırat

A thesis submitted to the

University of Colorado in partial fulfillment

of the requirements for the departmental honors

Bachelor of Arts

Department of Physics

2019

This thesis entitled:
Local Holographic Superconductors and Hovering Black Holes
written by Atakan Hilmi Fırat
has been approved for the Department of Physics

Associate Prof. of Physics Oliver DeWolfe

Prof. of Physics John Cumalat

Prof. of Physics Thomas DeGrand

Prof. of Mathematics Jeanne Clelland

Date

The final copy of this thesis has been examined by the signatories, and we find that both the content and the form meet acceptable presentation standards of scholarly work in the above mentioned discipline.

Fırat, Atakan Hilmi (B.A., Physics)

Local Holographic Superconductors and Hovering Black Holes

Thesis directed by Associate Prof. of Physics Oliver DeWolfe

Understanding the behavior of the high-T_c superconductors is among the most important open questions in physics where many conventional field theoretical methods fail due to strong interactions of electrons. Recent advancements in string theory and holographic dualities that map $d+1$ dimensional quantum field theories in strongly coupled regimes to $d+2$ dimensional weakly curved classical general relativity proved to be useful for understanding the high-T_c superconductivity behavior. It is shown that the general properties of so-called "holographic superconductors" of the field theory side can be extracted by investigating the "hair" of the charged scalar field around the black hole in the Anti-de Sitter background. In this thesis, I numerically construct the gravitational duals of local electrically charged defects, modeled by various spherically symmetric chemical potential profiles in the boundary, when the charged scalar instabilities are presents at finite temperatures, in order to model local holographic superconductivity behavior. My research investigates the behavior of the superconducting order parameter and the critical temperature T_c under the presence of such defects, and compare it with the global holographic superconductors. Also, my research investigates the physics of hovering black holes, which these types of systems are known to include.

Acknowledgements

I would like to thank Oliver DeWolfe for being an excellent advisor and helping me throughout the process of writing this thesis. I also would like to thank Tomas Andrade for sharing his code and lecture notes on holographic lattices, which helped me to improve my understanding of applied holography immensely.

Lastly, I would like to extend my gratitude to my family and friends, without whom writing this thesis would be unimaginable.

Contents

Tables

Table

Figures

Figure

Chapter 1

Introduction

1.1 High-T_c Superconductors and Strange Metals

Understanding the physics of high-T_c superconductivity, such as the one that is observed in cuprates [31], shown in figure (1.1), is one of the many open questions in the theoretical condensed matter physics. However, because of the strong interactions of electrons and lack of apparent quasiparticles in these systems, the usual field theoretical methods, such as naive perturbation theory, often fails. As a result, physicists have employed various and sophisticated techniques, ranging from numerical simulations to gravity [13, 18, 19, 20], in order to understand the behavior of these systems.

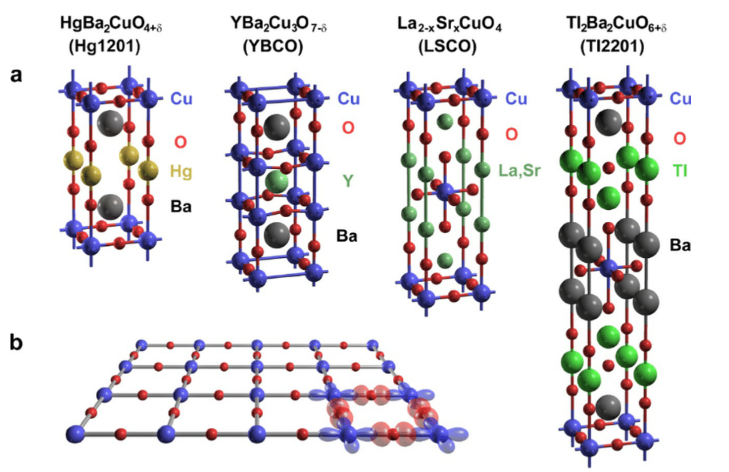

Figure 1.1: The chemical composition of cuprates: a) The chemical composition of various cuprates, b) 2-dimensional copper-oxide plane in cuprates which is thought to be where superconductivity takes place, see [31]. Figure is taken from [4].

At the time of writing this thesis, the normal phases of these superconductors, known as *strange metals* or *non-Fermi liquids*, are thought to be at the finite density but lack a sharp Fermi surface by theoretical motivations and experimental evidences [36]. This behavior is in contrast to the normal phases of BCS superconductors which have a clearly defined Fermi surface. It is believed that these strange metal phases might occur because of a quantum critical point at the zero temperature, which impacts the finite temperature physics and making it a critical phase as well [36]. It is thought that upon this quantum critical phase, superconductivity forms.

After assuming that the normal phase of high-T_c superconductors behaves critically, a natural question one might ask is what happens when we add a certain defect or disorder to this system. Obviously, superconductivity would be effected by the presence of such defects, because the defect would modify the local charge density around it nontrivially. However, since there is no Fermi surface in these phases, it is reasonable to think that the resulting effects would be widely different from conventional superconductors. Also, inspiring from the common wisdom in the condensed matter community regarding strong interactions, one might argue that this behavior might make the system behave counterintuitively. For instance, it might make superconductivity more robust in certain regimes and/or for certain types of defects.

Hence, the motivation behind this study is to understand, both quantitatively and qualitatively, how such impacts of defects and disorder change the physics of these systems, focusing on the superconductive behavior and its critical temperature.

1.2 Why String Theory and Gravity?

In order to address the physics of high-T_c superconductors as mentioned in the previous section, we must have some kind of mathematical framework in our toolbox to understand, and most importantly calculate, what is going on. In this study, this framework would be provided, maybe surprisingly, by the general theory of relativity and string theory.

It is a well-established fact that the general theory of relativity works perfectly as a theory of classical gravitation. However, with the advancement of string theory, especially with the formulation of the Maldacena conjecture nearly two decades ago [29], we now have a more detailed answer regarding its dynamics and general relativity is no longer limited to the realm of astrophysics, but touches nearly every sub-discipline of physics.

One of the unexpected applications that general relativity enjoys can be found in condensed matter physics via holography. It is now well-established that the physics of certain scale-invariant field theories in condensed matter physics in $d+1$ dimensions are extremely similar to the physics of classical gravity of $d+2$ dimensional spacetime with a negative cosmological constant [20]. Because of appearance of one more dimension, this approach named as holography: Gravity is a "hologram" of the condensed matter system.

This mysterious duality stems from string theory and one of the non-perturbative objects that it contains: *D-branes* [32]. However, as we will see in the literature and in this thesis, the "top-down" nature of such dualities often complicates the physics we try to extract unnecessarily without providing too much calculable content from the application point of view. As a result, using general theory of relativity with some additional matter fields is sufficient, provided that the cosmological constant is negative and gravity lives in one more dimension than the field theory. This approach often denoted as *bottom-up* in the holography literature [36], and this is the strategy we will employ throughout this study.

For our systems of interest, namely superconductors that forms on top of charged defects at finite temperature, we will discover that there is a natural way to incorporate them to the gravity side of the duality. We will explicitly construct such gravitational "duals" of condensed matter systems by solving the relevant Einstein Field Equations coupled to matter fields, such as electromagnetic and charged scalar fields. Then we will extract the relevant physics using previously established so-called "Anti-de Sitter/Conformal Field theory (AdS/CFT) dictionary" [36].

Along the way, we will encounter a novel type of black hole in AdS spacetime, known as *hovering black holes*, first observed in [24] and further developed in [27]. These systems are interesting for their own reasons,[1] but we will try to understand their meaning from the condensed matter

[1] For example, for its relation with the weak gravity conjecture, see [9].

point of view, especially when the superconducting order and the corresponding scalar hair of the black hole is present in the spacetime. Lastly, we will comment on the possibility of existence of a hovering black hole whose horizon topology is planar, rather than spherical like those in [24], and comment on some of its rather extraordinary implications to the field theory side that has no analog in the weak coupling.

Chapter 2

Holographic Duality

In this chapter, we introduce the physics of holographic duality which is the main component in our study. We first briefly describe some of the preliminary physics needed to understand the duality, namely Anti-de Sitter (AdS) spacetime, its black holes that will be used in this thesis, and conformal field theory (CFT). Then we show how AdS/CFT correspondence comes into being using string theoretical arguments from D-branes and its inner workings, and discuss its limits, properties, and appearance of an *extra dimension*. Below we work in the natural units where $\hbar = c = 1$, Einstein summation convention is assumed and $\eta_{\mu\nu}$ is taken to be the metric for $d+1$ dimensional flat spacetime with the convention $\eta_{\mu\nu} = \mathrm{diag}(-1, 1, \ldots, 1)$, for $\mu, \nu = 0, \ldots, d$. We will state explicitly if we use it differently from our convention.

2.1 Anti-de Sitter (AdS) Spacetime and Black Holes

Begin with considering Einstein Field Equations with a negative cosmological constant $\Lambda < 0$ and without any matter fields in $d+2$ dimensions, (i.e. $T_{\mu\nu} = 0$, and here $\mu, \nu = 0, \ldots, d+1$),

$$R_{\mu\nu} - \frac{1}{2} R g_{\mu\nu} + \Lambda g_{\mu\nu} = 0. \tag{2.1}$$

It is a straightforward exercise to show that the following metric satisfies this set of equations [1]:

$$ds^2 = \frac{L^2}{z^2}\left(dz^2 + \eta_{\mu\nu} dx^\mu dx^\nu\right). \tag{2.2}$$

This is the metric for *Anti-de Sitter (AdS) spacetime* written in the so-called *Poincare patch*. Here, $L = \sqrt{-\frac{d(d+1)}{2\Lambda}}$ is the relevant length scale in the AdS spacetime, denoted as *AdS radius*, which we will eventually set to 1. This spacetime is often denoted as AdS_{d+2}.

It is easy to show that AdS spacetime is a maximally symmetric spacetime with the isometry group $\mathrm{SO}(d+1,2)$ [1]. Note that this metric is invariant under scaling of coordinates, $(x^\mu, z) \to (\lambda x^\mu, \lambda z)$, where $\lambda > 0$ is some constant.

Also note that the metric (2.2) blows up as $z \to 0$. We will call this region the *asymptotic boundary*. Observe that at the asymptotic boundary the metric takes the form $ds^2 \sim \eta_{\mu\nu} dx^\mu dx^\nu$ asymptotically, which is the metric for $d+1$ dimensional flat spacetime and clearly describes a timelike surface since its normal is spacelike everywhere on this surface. This justifies our usage of Poincare patch, instead of other patches of AdS or global AdS, since, as we will see, corresponding condensed matter systems can be thought of as living in the boundary of AdS spacetime and we want these systems to be in the flat spacetime.

Lastly, observe that we can consider $d+2$ dimensional AdS spacetime, written in the patch above, as a stack of $d+1$ dimensional flat spacetimes curving in along the z direction. Looking forward to section (2.6), this is an important observation, since it will give a natural interpretation for the geometrization of the renormalization group in the holographic context.

Another solution to the equation (2.1) is *(planar) AdS-Schwarzschild black hole* whose metric in the Poincare patch is given by [1]

$$ds^2 = \frac{L^2}{z^2}\left(-f(z)dt^2 + \frac{dz^2}{f(z)} + d\vec{x}^2\right), \tag{2.3}$$

where $f(z)$ is the so-called *emblackening factor*

$$f(z) = 1 - \left(\frac{z}{z_+}\right)^{d+1}, \tag{2.4}$$

and z_+ is the position of the horizon which satisfies $f(z_+) = 0$. We denoted d spatial coordinate transverse to z collectively as $\vec{x}$ and we will keep this notation. Temperature of this black hole is

$$T = \frac{d+1}{4\pi z_+}, \tag{2.5}$$

which can easily be found by demanding regularity at the horizon $z = z_+$. Observe that in the limit of $z_+ \to \infty$, i.e. in the limit where the metric approaches to the metric (2.2), we would have $T \to 0$, so we can interpret the metric (2.2) has zero temperature. These points regarding temperature will be important later on, which we will derive them in the section (2.7) below.

Additionally, if we couple gravity to the electromagnetic field we would get the equations of motion for the Einstein-Maxwell Theory (here $\mu, \nu = 0, \dots, d+1$)

$$R_{\mu\nu} - \frac{1}{2} R g_{\mu\nu} + \Lambda g_{\mu\nu} = \frac{8\pi G}{e^2} \left(F_{\mu}{}^{\rho} F_{\nu\rho} - \frac{1}{4} g_{\mu\nu} F^{\mu\nu} F_{\mu\nu} \right), \tag{2.6}$$

$$\nabla_{\mu} F^{\mu}_{\ \nu} = 0. \tag{2.7}$$

Again, it is a trivial pursuit to check that (2.3) is a solution to the equations above, but with a slightly altered emblackening factor [1]

$$f(z) = 1 + Q^2 z^{2d} - M z^{d+1}, \tag{2.8}$$

where Q and M are two independent parameters. Additionally, we now have a nontrivial gauge field

$$A = \mu \left(1 - \left(\frac{z}{z_+} \right)^{d-1} \right) dt. \tag{2.9}$$

Here z_+ is the outer horizon distance, which is the smallest z that satisfies $f(z) = 0$ and μ is given by the relation

$$\mu = \sqrt{\frac{d}{8\pi G(d-1)}} e Q z_+^{d-1}. \tag{2.10}$$

This black hole is called *(planar) AdS Reissner-Nordström (AdS-RN) black hole.*

Again, by demanding regularity at the outer horizon $z = z_+$, we can read the temperature of this black hole, which equals to

$$T = \frac{d+1}{4\pi z_+} \left(1 - \frac{d-1}{d+1} Q^2 z_+^{2d} \right). \tag{2.11}$$

An AdS-RN black hole is said to be *extremal* if the term in the parenthesis above vanishes. In this case, temperature vanishes, $T = 0$, but there is still a charged horizon present in the AdS spacetime, since $z_+ \neq 0$ still. Physically, if a black hole is extremal, it can be shown that all of its energy is provided by electromagnetic field [36]. We will see how this black hole is related to the strange metal phases in a surprising fashion.

2.2 Conformal Field Theory (CFT)

Simply put, a conformally symmetric quantum field theory is called *conformal field theory*, often abbreviated as CFT. We can think conformal symmetries as any transformation that preserves the angles, but not necessarily the lengths. More precisely, CFTs are invariant under the transformations $x \to x'$ for which

$$g_{\mu\nu}(x) \to g'_{\mu\nu}(x') = e^{-2\omega(x)} g_{\mu\nu}(x). \tag{2.12}$$

The group of such transformations is $\mathrm{SO}(d+1,2)$ for $d > 1$ [1]. Note that this is the same as the isometry group of AdS spacetime in the section (2.1) above. This will be a useful observation when we map the symmetries and representations in two theories to each other in the section (2.7) below.

In this thesis, "heavy" machinery involving CFTs, such as conformal algebra or primary fields, is neither required nor desired. But in passing, it is useful to list certain properties of CFTs that will come in handy later on when we are building our model of local holographic superconductivity in section (3.3). For expanded discussion from the perspective of AdS/CFT correspondence, see [1].

- First of all, CFTs are scale-invariant theories. This implies that they can't have a mass gap, otherwise this scale invariance would be violated. In other words, all excitations are massless. So truly, degrees of freedoms in CFTs are not like particles but more like a "soup".

- The scale invariance of CFTs holds not only at the classical level but at the quantum level as well. As a result, it is required that beta function of CFTs vanish, $\beta(\lambda(\mu)) = 0$ at every energy scale μ. This will provide us a good playground to make the theory flow to a nontrivial low-energy regime by adding relevant operators. For instance, we can consider CFTs at finite density and ask what happens in the low-energy regime of the theory, as we will do later when we're considering gravitational duals of strange metals.

- Because of the high number of symmetries, the correlators of CFTs are highly constrained.

For instance, consider a scalar operator $\mathcal{O}(x)$ with the property $\mathcal{O}(\lambda x) = \lambda^{-\Delta}\mathcal{O}(x)$. Such operators are said to have *conformal dimension* Δ. Its two-point correlation function is given by

$$\langle \mathcal{O}(x)\mathcal{O}(0)\rangle = \frac{C}{|x|^{2\Delta}}, \tag{2.13}$$

where C is some constant. This form is completely fixed by the symmetries of the conformal group: The two-point correlation function can only depend on the distance between two points, $|x|$, by the Lorentz invariance, and this functional form is the only form that is invariant under scaling of $\mathcal{O}(x)$. As we will see, the order parameter for superconductivity in CFT will be a some operator of this type.

- It is believed that every scale-and Poincare-invariant theory is conformally symmetric [20]. Therefore, we are going to use scale invariance and conformal symmetry interchangeably throughout this study.

2.3 AdS/CFT Correspondence

Having described what "AdS" and "CFT" mean in the sections (2.1-2.2) above, we can now focus on the correspondence between these two, which will enable us to solve condensed matter problems with gravity. Here, we opt to present the most well-known and studied version of the duality, namely the correspondence between Type IIB closed superstring theory in $\mathrm{AdS}_5 \times \mathbb{S}_5$ background with $\mathcal{N} = 4$ SU(N) superconformal Yang-Mills (SYM) theory in $3+1$ dimensions [29]. For most of the bottom-up purposes, the exact formulation and the matter content of these two theories hardly matters, besides one of them is AdS_{d+2} and other one is CFT in $d+1$ dimension, but it is instructive to know how the argument for holographic duality runs, at least heuristically. Let g_s be the dimensionless string coupling constant and let l_s be the length of the string below.

The physics of *Dp-branes* lies at the heart of AdS/CFT correspondence. These are basically examples of non-perturbative objects in string theory that are extended in p spatial dimensions [32]. For our example above, we will consider the case of $p = 3$ and N of them stacked on top of each other, which can be realized in Type IIB superstring theory in flat background.

Now consider the low-energy regime of the system of N Dp-branes. In this regime, there are two ways to view the physics of Dp-branes, depending on the coupling constants and the number N. We can determine this dependence as follows. Since there are N Dp-branes and each one of them contributes g_s^{-1} to the total energy in the leading order, the energy of N Dp-branes goes like $E \sim \frac{N}{g_s}$ [20]. At the same time, the strength of gravity goes like g_s^{-2} for tree level [20]. Therefore, by multiplying these two, we can find the quantity $\lambda = 4\pi g_s N$ determines how strongly these objects gravitate: If $\lambda \gg 1$ the gravitation is strong and vice-versa, when $\lambda \ll 1$ it is weak. Here we add 4π because of conventions.

So, considering the limit $l_s \to 0$ and $N \to \infty$ for technical purposes, we have two different behaviors for the low-energy excitations,

- When $\lambda \gg 1$, N Dp-branes gravitate strongly. In this regime, we ought to consider this system as a black brane (planar black hole) in $9+1$ dimensions, since Dp-branes collapse onto each other gravitationally. It is found that the system decouples into two parts, Type IIB supergravity on $\mathrm{AdS}_5 \times \mathbb{S}_5$ background with Type IIB supergravity theory in $9+1$ dimensional flat space [29]. Here, the radius of AdS and sphere are both equal to L and they are related to the string length by $L = \lambda^{1/4} l_s$, which is finite and non-zero in the limits we are working in, see [20].

- When $\lambda \ll 1$, N Dp-branes do not gravitate and can be thought of as a plane in which strings can end [32].[1] In this case it is found that the low-energy excitations of N Dp-branes correspond to $\mathcal{N} = 4$ SU(N) superconformal Yang-Mills theory in $3+1$ dimensions, by considering strings stretching between the branes, along with the decoupled Type IIB supergravity theory in $9+1$ dimensional flat space [29]. Here, it is found that the coupling constant of SYM theory is related to the string coupling constant by $g_{YM}^2 = 2\pi g_s$ [20].

Observe that the latter of the decoupled theories in both of the cases is Type IIB supergravity

[1] Because of this boundary condition on open strings "D" in D-branes stands for Dirichlet.

theory in $9+1$ dimensional flat space. The degrees of freedom of this theory interpolates between big and small λ, (i.e. for any λ degrees of freedom remain independent from other theory) so that the other side of the decoupled theories are mapping into each other [20]. That means Type IIB supergravity in $\mathrm{AdS}_5 \times \mathbb{S}_5$ background and $\mathcal{N} = 4$ SU(N) superconformal Yang-Mills theory in $3+1$ dimensions are equivalent for $N \to \infty$, with the certain equivalence between their coupling constants and parameters discussed in [20]. This conjecture is believed to hold for not only low energy but all the regimes. So we can replace "supergravity" with "superstring theory" above and drop the requirement for $N \gg 1$ [1].

At this point, it is useful to establish some terminology. We will often call AdS spacetime *gravity side* or *bulk* and CFT *field theory side* or *boundary.* The latter terminology would be clear when we consider properties of the correspondence, which we will do after the discussion of the limits of the duality.

2.4 Limits of AdS/CFT

Often times in physics we have to take some limits to calculate what we want and AdS/CFT correspondence is no exception. In its full glory, called *the strongest version*, it is a nontrivial statement about the dynamics of quantum gravity in certain backgrounds, however, it is often too hard in this case to do an explicit numerical or analytical calculations for the field theory side using gravity.

Moreover, we would like to understand strongly coupled quantum field theories (QFTs), therefore the first thing we need to do is make the field theory side strongly coupled in some sense. We can take $g_{YM} \to \infty$ naively, however, note that this would also make $g_s \gg 1$ (see section (2.3)), which is not useful for practical purposes, since it will take us outside of the perturbative regime of string theory, which we know so little about.

Another way to make the field theory strongly coupled is to take the so-called *large-N* limit, that is taking $N \to \infty$ while keeping $\lambda = 4\pi g_s N$ finite. In this limit, we see the gravity side reduces to classical string theory since $g_s \to 0$, so effectively there is no quantum correction, i.e.

loop diagrams in string theory (that is Riemann surfaces with holes) are suppressed. This version of the duality is called *the strong form* [1].

In this limit, it is discovered that degrees of freedom have been organized with the new coupling constant $\lambda = 4\pi g_s N$ in the field theory side by 't Hooft [22]. So, by taking $\lambda \to \infty$, we can get strong coupling in the field theory side at large-N limit. Furthermore, by taking this limit, we get $L \gg l_s$, which effectively turns strings to point particles and reduces the gravity side to a classical, weakly-coupled supergravity, by the relations we established the section (2.3) above. This version, denoted as *the weak form* [1], is the limit we are going to use throughout this paper.

Using this logic, we established that some strongly coupled QFT is equivalent to some classical, weakly curved gravitational theory in one more dimension with a negative cosmological constant, which we can use perturbation theory for, at the cost of making the number of degrees of freedom, N, large. In practice, there might be some issues regarding this limit, which is in some sense like a thermodynamic limit. However, so far it is observed that large-N limit is working unreasonably well for the range of problems both in the duality itself and in the applications to condensed matter theory [36], and it is a mystery by itself why it is working so well. In any case, it is a good practice to be aware of this limit when we're doing physics and we will note when it might possibly cause trouble.

One last thing we need to illuminate regarding the nature of the duality is how we can apply the physics of highly symmetric system, such as supersymmetric, conformal Yang-Mills theory as we have seen above, to the field theories of condensed matter physics, for which the number of symmetries are often limited. There is a twofold answer for this. First, in practice, these high number of symmetries would be broken by the effects of the chemical potential and/or other operators and they won't survive in the low-energy limit of the theory, which is what we care in the condensed matter theory.

Second, the correspondence between AdS and CFT is believed to hold for not only very specific theories like above, but *in general* [36]. That is, we can find a gravitational AdS dual for any given CFT and vice versa. In the bottom-up approach, this is usually one's starting point.

Hence, this more general understanding of the duality is sometimes called *holographic duality* or *gauge/gravity duality*. We will use all of these terms interchangeably throughout our study.

2.5 Properties of Holographic Duality

Some of the reasons why we are interested in the holographic duality are listed in the sections above. Here we will expand some of the points we made in more detail.

First and foremost, it is useful to emphasize again that holographic duality is a *strong/weak duality*: It maps a weakly coupled, classical gravitational theory to a strongly coupled quantum field theory [20]. In some sense, all of its power stems from this fact, because it enables us to look at quantum field theory nonperturbatively by doing perturbative gravitational calculations. Also, it is a duality between a quantum and a classical theory [20], which helps us understand quantum effects just by considering a classical theory without considering any complications because of the quantum nature (but with the possible complications of classical gravity, such as nonlinearity).

Secondly, we have already noted the isometry group of AdS and the global symmetry group of CFT are the same group, namely $\mathrm{SO}(d+1,2)$ for $d>1$. This bring us to the fact that holographic duality is a *global/local duality*. Local symmetries of the gravity side, i.e. isometries, are mapped to the global symmetries of the field theory side [1]. Moreover, this equivalence of symmetries is not limited to the spacetime symmetries, but can be extended to the internal symmetries, such as U(1) symmetry [36]. That is, a global internal symmetry in the field theory side is mapped to the local gauge symmetry in the gravity side with the same group. This point will be expanded in section (2.7) once we establish the relation between the bulk and the boundary more precisely.

Now using the fact that symmetries map to each other, it is easy to map degrees of freedom of each of the theories as well. All we need to do is *dualize* the operator $\mathcal{O}$ in the field theory side with a field ϕ in the gravity side such that they are in the same irreducible representation of both $\mathrm{SO}(d+1,2)$ and the internal symmetry group, which we always take to be U(1) in this thesis. Therefore, $\mathcal{O}$ and ϕ should have the same tensor indices and their scaling behavior should be the same as we mentioned in the section (2.2) above (as well as charges if it is charged under internal symmetry).

We also need to have an explicit "master" equation for how these two objects relate to each other mathematically and the *GKPW rule* provides this [17, 35]. The GKPW rule is motivated by string theoretical top-down constructions, so we won't get into details how it comes into being. Assuming the operator $\mathcal{O}$ in the field theory side is dualized by the field ϕ in the gravity side, it relates the partition functions of the theories on both sides of the duality formally as

$$\int_{\phi\to J}[d\phi]e^{iS[\phi]_{AdS}} = \langle e^{i\int d^{d+1}xJ(x)\mathcal{O}(x)}\rangle_{CFT}\,. \tag{2.14}$$

Before moving on, note that by doing Wick rotation and taking the logarithm of both sides, this equation reduces to, in the classical limit of AdS spacetime,

$$\frac{F}{k_B T} = \log(Z_{CFT}) \approx -S_E[\phi_{sol}]. \tag{2.15}$$

Here F denotes the free energy of the given ensemble, T is temperature, and k_B is the Boltzmann constant (which we will set to 1 eventually). We related the free energy and the logarithm of the Euclidean partition function (which we simply denoted as Z_{CFT}) using statistical mechanics. Also note that ϕ_{sol} is the solution that satisfy the Euler-Lagrange equation, since at the classical level the logarithm of the partition function of AdS evaluates to the on-shell value of the action by usual path integral arguments [36]. What this equation means is that the free energy of the field theory can be found using the on-shell value of the Euclidean action of AdS spacetime. We will use this fact in chapter (5) later on when we try to check explicitly which solution dominates in the grand canonical ensemble.

Continuing on, the GKPW rule (2.14) implies that the asymptotic behavior of the field ϕ near the boundary provides a source for the operator $\mathcal{O}$ [20]. That is, if we have the following asymptotic expansion of the field ϕ in the AdS side at $z = 0$, assuming $\delta_1 < \delta_2$,

$$\phi(x^\mu, z) = \phi_0(x^\mu)z^{\delta_1} + \phi_1(x^\mu)z^{\delta_2} + \ldots, \tag{2.16}$$

we can take the leading coefficient of the expansion above to be the source for the operator $\mathcal{O}$, i.e $\phi_0(x^\mu) = J(x^\mu)$, in the field theory side.

Generally the exponents in the series above would be determined by the types of fields and masses of them, so indicate this dependency with $\delta_1 = \delta_1^{\phi}(m)$ [1]. Note that because of the scaling invariance of AdS spacetime, the solution for the field ϕ does not scale, i.e. $\phi \to \phi$. From this and by the first term in the expansion (2.16), we immediately see $\phi_0 \to \lambda^{-\delta_1^{\phi}(m)}\phi_0$ as a result. Similarly, assuming the operator $\mathcal{O}$ transform as $\mathcal{O} \to \lambda^{-\Delta}\mathcal{O}$ under scaling $x \to \lambda x$, we see its source scales as $J \to \lambda^{\Delta-d-1}J$.

Since we assumed that $\mathcal{O}$ and ϕ are dual to each other and we claimed that $\phi_0(x^\mu) = J(x^\mu)$ by the GKPW rule (2.14), their scaling behavior must be the same. That is, we need to have

$$\Delta - d - 1 = -\delta_1^{\phi}(m) \implies \Delta = d + 1 - \delta_1^{\phi}(m). \tag{2.17}$$

This shows that the conformal dimensions in the field theory side are related to the masses of the fields in the gravity side in a specific fashion. This relation, along with being in the same representation of the Poincare group and/or internal group as we noted above, allow us to relate the operators in the field theory and the fields in AdS spacetime to each other naturally. Some of these dualizations are summarized in the table below. We will mostly be interested in relating scalar operators in both sides together.

Operator in CFT	Field in AdS	Relation
Scalar Operator $\mathcal{O}^{\Delta}$	Scalar Field ϕ	$m^2L^2 = \Delta(\Delta - d - 1)$
U(1) Current J_μ	U(1) Gauge Field A_μ	$m^2L^2 = 0$ and $\Delta = 1$
Stress-energy Tensor $T_{\mu\nu}$	Metric $g_{\mu\nu}$	$m^2L^2 = 0$ and $\Delta = d + 1$

Table 2.1: The relation between some of the operators/fields in both sides. Here Δ denotes the conformal dimensions of the operators in CFT and m denotes the mass of the corresponding fields in the AdS. For detailed analysis, see [1].

Observe that we also kept the subleading term in the expansion (2.16) above. Coefficient of this subleading term corresponds to the vacuum expectation value (VEV) of the operator $\mathcal{O}$ up to some multiplicative constant. In other words, we have $\langle \mathcal{O}(x^\mu) \rangle \sim \phi_1(x^\mu)$. This relation immediately follows form the GKPW rule (2.14) by taking logarithmic functional derivative with respect to $J = \phi_0$ of both sides. We get

$$\langle \mathcal{O} \rangle = i \left(\frac{\delta S[\phi]_{AdS}}{\delta J} \right)_{\phi \to J} = i \left(\frac{\delta S[\phi]_{AdS}}{\delta \phi_0} \right)_{\phi \to \phi_0 z^{\delta_1} + \phi_1 z^{\delta_2} + \ldots} . \tag{2.18}$$

Here, there's a complication regarding the terms that are linear in ϕ_0, but it turns out they can always be canceled by adding suitable formally infinite boundary counterterms [20].[2] So, the next term in $S[\phi]_{AdS}$ is proportional to $\phi_0 \phi_1$ in general, which will give the result $\langle \mathcal{O}(x^\mu) \rangle \sim \phi_1(x^\mu)$. We will use this fact multiple times when we are investigating the charge density on the boundary or VEV of the order parameter of superconductivity.

2.6 Extra Dimension

Maybe one of the mysterious features of the holographic duality is the appearance of an extra dimension.[3] That is, AdS side has one more dimension than the CFT side. Henceforth, this extra dimension would be called *holographic direction* or *holographic dimension*.

We have already seen in the previous section (2.5) that the fields in AdS relate to the operators in CFT in a rigid fashion. The asymptotic dynamics of AdS fields near the boundary are the same as CFT. Intuitively, this suggests that we can think CFT lives in the boundary of the AdS spacetime.

In fact, this is part of a more general result. Holographic direction essentially parameterizes the energy scale of CFT [20]: As $z \to 0$, we approach to the high-energy/short-wavelength limit of CFT, colloquially known as *ultraviolet (UV) regime*. This limit fits our intuition regarding that CFT lives on the boundary of AdS which we had deduced from the GKPW rule (2.14).

Conversely, as $z \to \infty$ in AdS, we are integrating more and more microscopic degrees of freedom and looking into the low-energy/long-wavelength limit of CFT, colloquially known as the *infrared (IR) regime* and this region is often called *deep IR* in AdS. This correspondence physically makes sense if we think about the gravitational redshift [20]. If we look into deep IR from the boundary where the UV regime of CFT lives, we would see that the perturbations in AdS are

[2] As we will see in the next section, this is exactly analogous to the UV divergences in the usual field theory.
[3] We ignore the other compact dimension, such as $\mathbb{S}^5$ above, that multiplies AdS for a moment. We will return to this point at the end of this section.

redshifted relative to the similar perturbations at the boundary because of AdS compression. This redshifting effect is essentially taking the long-wavelength limit in the field theory.

For a better physical argument for the duality between the energy scale of CFT and the holographic direction, consider stacking CFTs living in $d+1$ dimensional flat spacetime in some direction transverse to its dimensions, name it z, and effectively creating a spacetime in one more dimensions.[4] However, make it so that as z grows, we continuously integrate out microscopic degrees of freedom of CFT. In other words, make it so that z parameterizes the energy scale μ of CFT as $z \sim \mu^{-1}$. By Poincare symmetry of CFTs in the transverse directions to the z, the metric of this spacetime takes the following general form:

$$ds^2 = f(z)dz^2 + g(z)\eta_{\mu\nu}dx^\mu dx^\nu, \tag{2.19}$$

where $f(z), g(z)$ are some functions to be determined.

Now recall that CFTs are also invariant under scaling of the type $x^\mu \to \lambda x^\mu$ and the constructed metric (2.19) above ought to obey that. Also recall that the beta function of CFTs vanish, as we noted in section (2.2). So when we scale the distances, not only should we take $x^\mu \to \lambda x^\mu$ but $z \to \lambda z$ at the same time. This is because of the fact that as we scale the lengths the energy should be scaled inversely (by dimensional grounds) to preserve $\beta = 0$, which results in the scaling $z \to \lambda z$.

This uniquely restricts the choice of metric to be

$$ds^2 = \frac{L^2}{z^2}\left(dz^2 + \eta_{\mu\nu}dx^\mu dx^\nu\right). \tag{2.20}$$

But this is no other than the pure AdS metric written in the Poincare patch. Note that this justifies why we had used the Poincare patch too again. Starting with a QFT in flat dimension and running this argument gave us AdS in the Poincare patch.

In a passing note, this interpretation justifies our usage of the *hologram*. In theory, every energy scale of CFT can be inferred from its UV by taking limits. As we showed, AdS is basically

[4] This discussion follows one that is made in [36].

constructed by combining CFTs at different energy scales by effectively adding one more dimension. So, forming the analogy that CFT is a 2D diffraction grating and AdS is the resulting 3D image, we see that we can think AdS as a "hologram" of CFT, hence the name holographic duality [36]. Additionally, in the limit we are working, CFT is complicated, like the actual shape of the diffraction grating, and AdS is simple, like the resulting image.

Having established the relation between the energy scale and the holographic dimension, we see that the information about renormalization group of a quantum theory has been geometrized, and it hasn't been geometrized by some arbitrary geometry, but in the borders of the general theory of relativity. This shows that understanding the gravitational dynamics in the holographic direction would be the same as understanding the renormalization group.

Moreover, by this connection, making CFT flow to a nontrivial IR by adding relevant operators becomes physically the same as changing the geometry of the deep IR region of AdS spacetime while keeping spacetime asymptotically AdS. So this, combined with the notion of *strong emergence* or *UV independence* [36], we can engineer specific IR fixed points for our purposes by finding suitable asymptotically AdS spacetime that dualizes the low-energy physics we want to probe.

The idea of the strong emergence basically comes from the Wilsonian idea of renormalization: Our starting theory for the short-distance physics shouldn't matter for the long-distance physics. Therefore, in theory, as long as we can produce the same IR from two completely different high energy theory it shouldn't matter what we use for it, the degrees of freedoms in the higher scale will decouple from lower ones in any case.

So, in the context of holographic duality, we can replace, say strongly coupled Hamiltonian of electrons in cuprates with some CFT with additional operators (such as the chemical potential as we will see) so that we have the similar low-energy physics in both cases. Then knowing that the physics is dualized by gravity, we can acquire information regarding low-energy field theory nonperturbatively using general relativity. This is the heart of research program of holographic duality and its application to condensed matter physics, known as Anti-de Sitter/Condensed Matter Theory (AdS/CMT) correspondence.

Lastly note that, we should account for the compact dimensions that generally multiply AdS to completely cover all of extra dimensions. However, their effect on AdS would be just the addition of extra fields by Kaluza-Klein dimensional reduction [1], which we emphasized that they don't matter for our purposes. So they won't alter the bottom-up discussion we would make in the next chapters.

2.7 AdS/CFT Dictionary

In the sections (2.5) and (2.6), we have discussed how some of the physical observables in both sides are equivalent, or *dualized*, to each other. For example, we have discussed how local gauge symmetries in AdS spacetime are dual to the global symmetries of the same type in the corresponding CFT.

Let's make this relation between symmetries clear by considering a U(1) gauge field in AdS, A_μ. It has a gauge freedom $A_\mu \to A_\mu + \nabla_\mu \chi$ as usual. Here $\chi = \chi(x^\mu, z)$ is a spacetime dependent parameter. Considering only the asymptotic flat boundary of AdS, this gauge field will couple to some field J_μ, and this term will transform under gauge transformation as follows [20]:

$$\int_\partial d^{d+1}x A_\mu J^\mu \to \int_\partial d^{d+1}x \left(A_\mu + \partial_\mu \chi\right) J^\mu = \int_\partial d^{d+1}x \left(A_\mu J^\mu - \chi \partial_\mu J^\mu\right). \tag{2.21}$$

In the last step we integrated-by-parts and ignored the boundary terms. Note that this term ought to be gauge invariant, so we must have $\partial_\mu J^\mu = 0$. This shows that J^μ conserved at the boundary, hence there should be a conserved current in CFT. This is an indicator of a global symmetry in CFT, in this case it is naturally U(1) global symmetry. This relation can be applied to any gauge symmetry, including diffeomorphisms, showing that the symmetries in both sides are indeed mapping to each other.

In general the physical observables are mapped to each other in "natural" fashion under holographic duality, like symmetries do, as we showed above. We won't go over how each of these maps are constructed. We refer the reader to the excellent literature for how these rules are derived, see [1, 11, 20, 30, 36]. These rules are collectively known as *AdS/CFT dictionary.*

However, we will quickly go over some of the important features of the dictionary which we will use later on. First, we see that temperature of a black hole is mapped to temperature of the dual CFT [20]. This entry in the dictionary basically comes from demanding regularity for the black hole horizon in AdS. Say we have a metric like in (2.3). Consider the Euclidean version of this metric with imaginary time $\tau = it$, and Taylor expand near the horizon $z = z_+$ to obtain the following metric

$$ds^2 = \frac{L^2}{z_+^2}\left(|f'(z_+)|(z_+ - z)d\tau^2 + \frac{dz^2}{|f'(z_+)|(z_+ - z)} + \dots\right). \tag{2.22}$$

Now by changing the coordinates $(z, \tau) \to (\rho, \varphi)$ where

$$z = z_+ - \frac{z_+|f'(z_+)|}{4L^2}\rho^2 \quad \tau = \frac{2}{|f'(z_+)|}\varphi, \tag{2.23}$$

the metric near the horizon becomes

$$ds^2 = d\rho^2 + \rho^2 d\varphi^2 + \dots. \tag{2.24}$$

Clearly, there shouldn't be any (conical) singularities at the horizon. That means the coordinate φ must be periodic with a period 2π. This gives

$$\varphi \sim \varphi + 2\pi \implies \tau \sim \tau + \frac{4\pi}{|f'(z_+)|}. \tag{2.25}$$

This result implies that the imaginary time is periodic, and note that it is periodic at the asymptotic boundary of AdS, where CFT lives, as well. It is a standard result of statistical field theory that the periodicity of imaginary time is given by inverse temperature.[5] Hence temperature of the field theory given by the presence of the black hole horizon is

$$T = \frac{|f'(z_+)|}{4\pi}, \tag{2.26}$$

which confirms temperatures (2.5) and (2.11). Interestingly, this temperature is found classically, but they match the semi-classical result of Hawking temperature of black holes. From this reasoning, we can say temperature of the black hole is mapped to temperature of the dual CFT. Additionally,

[5] We set the Boltzmann constant to 1, $k_B = 1$, for simplicity. We can rescale time coordinate to do that easily.

observe that for an extremal black hole horizon, the corresponding temperature vanish, and dual CFT is at zero temperature but still at finite density by having a nonvanishing temporal gauge field as we show now.

The second important point is that the presence of an electric potential in AdS means that we have a chemical potential μ in CFT [20]. This is easy to see, as we showed above current J_μ is dualized by the gauge field A_μ and having a chemical potential in the field theory side is simply adding the following term to the action of CFT:

$$S_{chem} = -\int_\partial d^{d+1}x(\mu\rho) = -\int_\partial d^{d+1}x(\mu J^0), \tag{2.27}$$

where $\rho = J^0$ is the charge density in CFT. By the duality, the coefficient of the leading term of $A^0 = -A_0$ at the boundary should provide the source for J^0, which is $-\mu$, so we see the gauge field in AdS must take the following form on the boundary:

$$A|_\partial = \mu dt. \tag{2.28}$$

This indicates there should be a nonvanishing electric potential in AdS and it corresponds to dual CFT having a finite (charge) density. The physics of the chemical potential is important, because it allows us to encode the finite density physics.

In fact, we have already encountered the case where the gauge field is present, AdS-RN black hole. It has temperature and a non-vanishing electric potential, so the corresponding CFT is at both finite temperature and density. Especially, the IR regime of such CFT is extremely interesting, it has been found that at low temperatures, $\mu \gg T$, the deep IR geometry takes the form AdS_2-Schwarzschild black hole times $\mathbb{R}^d$ [20].

To show this feature, first consider the extremal case, $T = 0$ but $\mu \neq 0$. Recall that in this case we have $1 - \frac{d-1}{d+1}Q^2 z_+^{2d} = 0$. This relation, combined with the fact $f(z_+) = 0 = f'(z_+)$, evaluates the emblackening factor (2.8) when $z \approx z_+$ by Taylor expansion

$$f(z) = 1 + \frac{d+1}{d-1}\left(\frac{z}{z_+}\right)^{2d} - \frac{2d}{d-1}\left(\frac{z}{z_+}\right)^{d+1} \approx d(d+1)\left(\frac{z-z_+}{z_+}\right)^2. \tag{2.29}$$

Then the metric (2.3) near the horizon becomes

$$ds^2 \approx \frac{L^2}{z_+^2}\left(-d(d+1)\left(\frac{z-z_+}{z_+}\right)^2 dt^2 + \frac{dz^2}{d(d+1)\left(\frac{z-z_+}{z_+}\right)^2} + d\vec{x}^2\right) \tag{2.30}$$

$$= \frac{L_2^2}{\zeta^2}\left(-dt^2 + d\zeta^2\right) + d\vec{y}^2. \tag{2.31}$$

Here we defined the ζ, $\vec{y}$, and L_2 as follows:

$$\zeta = \frac{z_+^2}{z_+ - z}\frac{1}{d(d+1)}; \quad \vec{y} = \frac{L}{z_+}\vec{x}; \quad L_2 = \frac{L}{\sqrt{d(d+1)}}. \tag{2.32}$$

Similarly when $z \approx z_+$ the gauge field (2.9) becomes

$$A \approx \mu(d-1)\frac{z_+ - z}{z_+}dt = \sqrt{\frac{d(d+1)}{8\pi G}}e\frac{z_+ - z}{z_+^2}dt. \tag{2.33}$$

Observe that by the metric (2.31), spacetime has the topology $\mathrm{AdS}_2 \times \mathbb{R}^d$ near the horizon. Why does this matter? Consider the scaling behavior in this region. The metric (2.31) is invariant under the transformation $(\zeta, t, \vec{y}) \to (\lambda\zeta, \lambda t, \vec{y})$ as can be easily seen. By introducing the parameter *dynamical critical exponent* z (not to be confused with the holographic direction), we can write the scaling of time and spatial coordinates in the following suggestive manner

$$t \to (\lambda^{1/z})^z t = k^z t \quad \vec{y} \to \lambda^{1/z}\vec{y} = k\vec{y} \quad \text{as} \quad z \to \infty. \tag{2.34}$$

Above we also introduced a parameter $k = \lambda^{1/z}$.

In the condensed matter literature, such scaling behavior is called *local quantum criticality* [36]. It is local in the sense that while the spatial directions do not scale, time scales infinite-fold. It has been suggested empirically that such a purely temporal critical behavior might be similar to the physics of strange metals [14, 36].

Moreover, we see that AdS spacetime has produced an *emergent* scaling behavior in the *IR* which is suspected to carry very similar low-energy physics with strange metals, by the quantum criticality we will discuss in the next chapter [14, 20]. All we needed to do was consider strongly coupled large-N CFT at finite density and zero temperature, and in the end it didn't matter which Hamiltonian we started with. This is precisely the reason why holographic duality gives us a gateway to understand the physics of strange metals. From now on, we can just consider AdS-RN black hole and solve for observables gravitationally and carry it into the field theory side with AdS/CFT dictionary to make predictions/postdictions for strange metals.

Additionally, in the low temperatures $T \ll \mu$, it is not hard to show that we produce AdS$_2$-Schwarzschild black hole times $\mathbb{R}^d$, with the similar reasoning [20]. Also note that as temperature grows, the horizon of black hole also grows as well, which eventually "eats" this deep IR region. This is the same physics as the suppression of the scaling behavior at higher temperatures in field theory. We won't repeat it here, but it is important to know this for our purposes.

Lastly, we will briefly mention objects for which Wilson loops in the field theory corresponds in the gravity side, since it will be a useful tool to understand the effects of hovering black holes to the field theory side. It has been suggested that the Wilson loops are dualized by the string worldsheet that minimizes its surface area in AdS with its boundary shaped as the dual Wilson loop [1].

It has been found that if the top of the string worldsheet is connected when it is dipped down in the AdS, it is an indicator for the confinement and vice versa, when the top becomes disconnected it indicates deconfinement [36]. As we will see, this fact might give an interesting result when we consider Wilson loops in disordered chemical potentials.

Chapter 3

Holographic Models of Superconductivity and Charged Defects

In this chapter, we describe the holographic models of superconductivity [18, 19, 23] and charged defects [9, 24, 27]. We mostly focus on what we call *global* holographic superconductors, for which superconductivity is formed on top of the constant and global chemical potential μ. First, we will describe strange metals and how superconductivity is thought to be formed on top of them. Then we will describe the general features of holographic superconductors. Lastly, we will review the physics of charged defects in the holographic context.

3.1 Superconductivity

Before we start, we should note that the aim of the holographic models of superconductors is to describe non-BCS superconductors *effectively.* That means most of the time we will ignore the microscopic physics, such as pairing mechanism, and focus more on macroscopic features. Unlike BCS superconductors for which electron-phonon interactions mediate the electron pairing, the pairing mechanism in the high-T_c superconductors is not clear at the time of writing this thesis. Some suggestion are given in [31].

Having said that, phenomenological theories of superconductors usually start with introducing an *order parameter*, Φ, a complex field which has a non-zero vacuum expectation value when superconductivity forms. This field can in general be a tensor, however to simplify the physics we will take it to be a scalar. Superconductors with a scalar order parameter is called *s-wave superconductors.* In cuprates, it is established that the superconductivity is a *d-wave* (i.e. the order parameter is rank-2 tensor) [31], but in practice including this would cause too much complication, especially in the holography context. We will comment on this issue later on.

In theory, the order parameter can be constructed from the microscopic degrees of freedom, if they are known. In BCS theory, for instance, the order parameter is simply given by the correlation functions of electron pairs. However, even in the case where the microscopic physics is not known or not clear, we can still write models with the order parameter. This phenomenological model of superconductivity is known as *Ginzburg-Landau Theory*, or its relativistic cousin, *Abelian-Higgs Model*, and it is based on the idea that superconductivity transition is a second-order, i.e. continuous, phase transition and happens because of the spontaneous symmetry breaking [36]. In the case of complex scalar order parameter, the broken group is U(1).

Now we will quickly sketch out how this theory works for the case of complex scalar order parameter Φ. Basically, the Abelian-Higgs Model states that the (Euclidean) action of the system can be written as follows [1]:

$$S_E = \int d^{d+1}x \left(\frac{1}{2} |\left(\partial_\mu - iqA_\mu\right)\Phi|^2 + \alpha(T)|\Phi|^2 + \frac{1}{2}\beta(T)|\Phi|^4 + \frac{1}{4e^2}F^2 \right). \tag{3.1}$$

As usual A_μ is the gauge field, $F_{\mu\nu} = \partial_\mu A_\nu - \partial_\nu A_\mu$ is the field strength, and $F^2 = F_{\mu\nu}F^{\mu\nu}$. For the existence of ground state, we have to take $\beta(T) > 0$.

We can easily see that the vacuum of the system is $\langle\Phi\rangle = 0$ when $\alpha(T) > 0$. The Abelian-Higgs Model states that there exists a critical temperature T_c such that $\alpha(T)$ changes sign, i.e $\alpha(T_c) = 0$, and $\alpha(T) < 0$ when $T < T_c$. Note that for temperatures $T < T_c$, the vacuum of the system then becomes $\langle\Phi\rangle = \sqrt{-\frac{\alpha(T)}{\beta(T)}}$, which means formation of superconductivity at temperature below the critical temperature in this picture. Note that this is extremely similar to the Higgs mechanism, and this shouldn't be surprising, since the same physics of spontaneous symmetry breaking is at work. So, by this wisdom, we can say what we call superconductivity is the spontaneous symmetry breakdown of the associated symmetry.

Also, considering the mean-field transitions, we find when temperature is sufficiently close to the critical temperature $T \approx T_c$, the order parameter scales as [36]

$$\langle \Phi \rangle \sim (T - T_c)^{1/2}. \tag{3.2}$$

Of course, considering one-loop corrections to this, we will renormalize the exponent to some value other than 1/2, depending on the universality class.

For our purposes, it is enough to know such description of superconductivity exists without going too much into details. However, we should note that we made a hidden assumption regarding the spatial dependence of the VEV of the order parameter Φ above. We assumed that it doesn't have any spatial dependence. However, in general, there might be some variation and it is a reasonable question to ask what happens in those cases, such as asking how the scaling of $\langle \Phi \rangle$ changes.

In the Abelian-Higgs model of superconductivity the answer is trivial, any spatial dependence of the VEV $\langle \Phi \rangle$ should add additional energy due to positive kinetic energy term contribution. However, in general, especially for the holographic models of superconductivity, we don't have clear cut answer like this because of subtleties associated with AdS spacetime. In the next chapters, we will answer this question in the context of holographic superconductors.

3.2 Quantum Critical Phases

Now we will describe the physics that is thought to be at work in strange metals in more detail. There is no point of telling the importance of the thermal phase transitions in physics. However, a phase transition might also occur because of quantum fluctuations rather than thermal fluctuations. In this case, we usually vary some parameter, say g, at zero temperature and at some $g = g_c$ the system undergoes a (second-order) phase transitions. Such transition points are called *quantum critical points* and these phase transitions are called *quantum phase transitions* [1]. Here critical denotes to fact that at this point the beta function of the theory vanishes and theory becomes scale-invariant, like in the thermal phase transitions.

We should note that by the same reasons for the case of the thermal phase transition, in the quantum phase transitions microscopic details are not important up to universality classes (they are “washed” away) and in general there’s no restriction for the strength of the critical point $g = g_c$. So in general these systems should be considered strongly coupled rather than perturbative.

Moreover, these quantum critical points leave an impact to the finite temperature physics [20]. We can see that by considering the dynamical scaling exponent z defined in section (2.7). By dimensional analysis, the correlation length ξ and the characteristic energy Δ of the phase transition with dynamic scaling exponent z should be related to each other as follows:

$$\Delta \sim \xi^{-z} \sim |g - g_c|^{z\nu}. \tag{3.3}$$

Above we use the fact that the correlation length is related to parameter g in the fashion $\xi \sim |g - g_c|^{-\nu}$, where ν is the critical exponent that depends on the system.

Now recall the usual interpretation of correlation length in the statistical field theory. It basically means that for the distances less than ξ, the system is critical. Similarly, we can also say, the system is critical for energies greater than the characteristic energy by dimensional analysis. So for the energies $T > \Delta \sim |g - g_c|^{z\nu}$., the system should still be critical. Such regions define a “wedge” in the phase space as shown in figure (3.1). These phases are then denoted as *quantum critical phases*. Lastly, observe that at finite temperatures we would have $\Delta \sim T$ near the transition, so they mark the boundaries of the edges of this wedge.

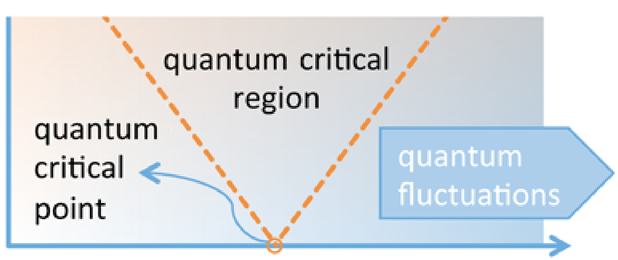

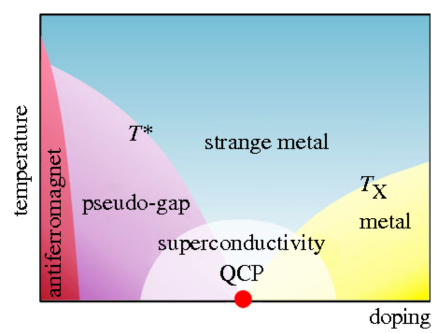

Figure 3.1: The generic phase diagram for quantum critical phase (left) and a sketch of experimentally observed phase diagram of cuprates (right). Figures are taken from [15, 28].

The experimental phase space diagram for cuprates is shown in figure (3.1) as well. Notice the similarity between the wedge of the quantum critical phase and the region for the strange metal, if we take coupling g above to be the doping. This is one of the indication that the quantum critical phases might at work in the strange metals. It is thought that a quantum critical point hides under so-called the superconductivity dome in cuprates [15].

Because of the physics quantum critical phases contains, namely strong-coupling, scale-invariant behavior, and its strong emergence from microscopic dynamics makes it a natural target for holographic duality. Because, as we saw in section (2.7), the similar physics can be found in the gravity side of the duality near the horizons of AdS-RN in deep IR. Hence, since the strange metal phase is believed to be in the subset of quantum critical phases, holographic duality can also be applied to the physics of strange metals. We should note that the analog of the doping (i.e. what we vary for quantum phase transition) in strange metals is the chemical potential in the gravity side. Again, we refer reader to the literature for many applications of this idea [20].

3.3 Holographic Superconductors

One of the distinguishing features of the two figures in (3.1) is the appearance of superconductivity in the phase diagram of cuprates for latter. Now we know that strange metal phases $\approx$ AdS-RN black holes, how should we account for this fact?

It turns out that there's a neat way to do that using holographic duality and again the symmetries will be our guide for constructing this model. For more details of these models, see [18, 19, 23]. Consider we have a CFT at finite density and temperature and correspondingly its gravitational dual AdS-RN black hole. Now assume there's a scalar order parameter $\mathcal{O}$ associated with the superconductivity and superconductivity results from spontaneous breakdown of *global* U(1) symmetry in the field theory side.[1]

How should one dualize that? From section (2.5), we know that the scalar order parameter $\mathcal{O}$ must be dualized by the scalar field Φ with a particular mass m related to the conformal dimension of $\mathcal{O}$. Additionally, we know that they must carry the same charge under U(1), so let it be equal to q.

[1] Because of the symmetry is global at the boundary, this would be a *superfluid* rather than a superconductor. However, we can promote it to be a superconductor by higgsing the global symmetry. We will keep this loose terminology which is shamefully common in the holography literature.

Therefore, our toy action in AdS must take the following form in order to model superconductivity:

$$S = \int d^{d+2}x \sqrt{-g} \left[\frac{1}{16\pi G} \left(R + \frac{d(d+1)}{L^2} \right) - \frac{1}{4e^2} F_{\mu\nu} F^{\mu\nu} - |(\partial_\mu - iqA_\mu)\Phi|^2 - V(|\Phi|^2) \right]. \quad (3.4)$$

Here, we assumed the scalar field minimally couples to gravity to keep the toy model simple and $V(|\Phi|^2)$ is the potential energy for the scalar field Φ. Near the transition temperature, we can ignore any self-interaction of the scalar field because of the physics of spontaneous symmetry breaking; higher order terms should be equal to zero. So it is sufficient to take the potential to be

$$V(|\Phi|^2) = m^2 |\Phi|^2 + \ldots. \quad (3.5)$$

Here dots means higher dimensional terms, which will be important away from the transition temperature. This choice, together with the action above is known as *minimal s-wave holographic superconductor* [36]. Before explaining the dual mechanism related to the superconductivity in the field theory side, observe that AdS-RN black hole is a solution to this action, together with $\Phi = 0$.

By varying the action (3.4) with respect to Φ and setting $\delta S = 0$, we get the following equation of motion, as one can easily check [16]

$$(\mathcal{D}_\mu \mathcal{D}^\mu - m^2)\Phi = 0, \quad (3.6)$$

where $\mathcal{D}_\mu = \nabla_\mu - iqA_\mu$ is the covariant derivative both in gauge symmetry and coordinate transformations. This is a linear equation, so consider perturbations of the scalar field on the AdS-RN black hole background, i.e. take $\Phi \to \delta\Phi$, and ignore the gravitational back-reaction of the scalar field, which is known as *probe-limit.* Only time component of the gauge field is non-vanishing in this background, $A_0 \neq 0$, as a result the equation of motion for the scalar perturbations $\delta\Phi$ takes the form

$$\left[\nabla^2 - \left(m^2 - q^2 |g^{00}| A_0^2 \right) \right] \delta\Phi = 0. \quad (3.7)$$

This is a Klein-Gordon-like equation in the background of AdS-RN black hole with the effective mass squared $m_{eff}^2 = m^2 - q^2 |g^{00}| A_0^2$. Note that we write the effective mass in this queer fashion to show explicitly $m_{eff}^2 \leq m^2$, since the second term is only composed by positive quantities.

Note that near the asymptotic boundary, $g^{00} \approx \frac{z^2}{L^2}$ and $A_0 \approx \mu$, so the effective mass is essentially $m_{eff}^2 \approx m^2 - \frac{\mu^2 z^2}{L^2} \approx m^2$. On the other hand, at the (extremal) horizon we have $g^{00} \approx \frac{z^2}{L^2 f(z)}|_{z \to z_+}$ where $f(z)$ near horizon is give by (2.29) and $A_0(z \approx z_+)$ is given by (2.33). Combining these we see the effective mass is constant near the horizon and equals to

$$m_{eff}^2 = m^2 - \frac{q^2 e^2}{8\pi G}. \tag{3.8}$$

Now we can describe the dual physics of superconductivity in the bulk theory. Recall that in the flat spacetime any particle with the effective negative mass squared will lead to tachyonic instabilities, since the particle has unbounded potential energy in those cases. It turns out there is an analog of the same instability in AdS spacetime discovered by Breitenlohner and Freedman. Their result states that the fields that satisfy *Breitenlohner-Freedman (BF) bound* are stable in AdS [6, 7]

$$m^2 L^2 \leq -\frac{(d+1)^2}{4}. \tag{3.9}$$

So unlike the flat spacetime, AdS can support negative mass squared fields if they are sufficiently small in their magnitude. Roughly, the reason for this is the additional gravitational compression provided by AdS spacetime.

So we see in order to Φ to be stable in the asymptotic AdS and properly dualize the order parameter, the effective mass must satisfy the inequality (3.9). However, the effective mass can violate the bound near the extremal horizon, where a new AdS_2 factor appears at small temperatures as we showed in the last chapter. So the scalar field would be unstable in deep IR if it satisfies the inequality

$$(m_{eff} L_2)^2 \approx (m L_2)^2 - \frac{q^2 e^2 L_2^2}{8\pi G} \leq -\frac{1}{4}. \tag{3.10}$$

Also recall we had different radius, L_2, for this deep IR AdS_2. This violation of BF bound in the deep IR would not lead to inconsistencies in theory because, as we will see, it will drive the theory to different IR, which will be superconducting.

As a result, we conclude that there's a window for which the scalar field is stable in UV while unstable in IR. That happens when the mass of the scalar field is in the range

$$-\frac{(d+1)^2}{4} \leq (mL)^2 \leq \frac{q^2 e^2 L^2}{8\pi G} - \frac{d(d+1)}{4}, \tag{3.11}$$

We find this range for extremal case(i.e. $T = 0$), but the same logic also applies non-extremal case but it is more cumbersome [20], which is usually investigated with numerics.

When the mass of scalar field enters this range of instability, which is usually achieved by decreasing the temperature, AdS-RN black hole goes under so-called *superradiant instability*, which discharges the black hole [36]. What happens is that the potential energy becomes unbounded from below in the deep IR similar to tachyonic instability in the flat space, so the vacuum begins to decay from $\langle\Phi\rangle = 0$ configuration by spontaneously producing pairs of positive and negative scalar particles of Φ. If black hole is positively charged, negative particles are attracted towards black hole, while positive particles are repulsed. With the introduction of these particles to the black hole, the charge of the black hole begins to decrease, i.e. black hole *discharges*.

Eventually, the system must find an equilibrium by completely discharging the black hole or sufficiently changing the geometry of deep IR so that the spontaneous pair production is no longer possible. Additionally observe that the repulsed positively charged particles cannot escape to infinity because of the gravitational pull of AdS toward to the horizon. So, in equilibrium, the scalar particles should be around the black hole and the vacuum must gain a new VEV which do not vanish, $\langle\Phi\rangle \neq 0$. This corresponds to formation of a so-called *scalar hair* around the black hole [18].

Remarkably, in asymptotically AdS spacetime well-known no-hair theorems for asymptotically flat spacetime do not hold and there is a rich structure of phase transitions of black holes. At the end of such instability on top of AdS-RN black hole, the solution of the action (3.4) found such that the scalar field can have a non-vanishing amplitude outside of the black hole. Typical solution would look like in the figure (3.2) below.

We should note that this hair is what encodes the superconductivity of the field theory side gravitationally. Recall that we can expand the scalar field near the asymptotic boundary in the

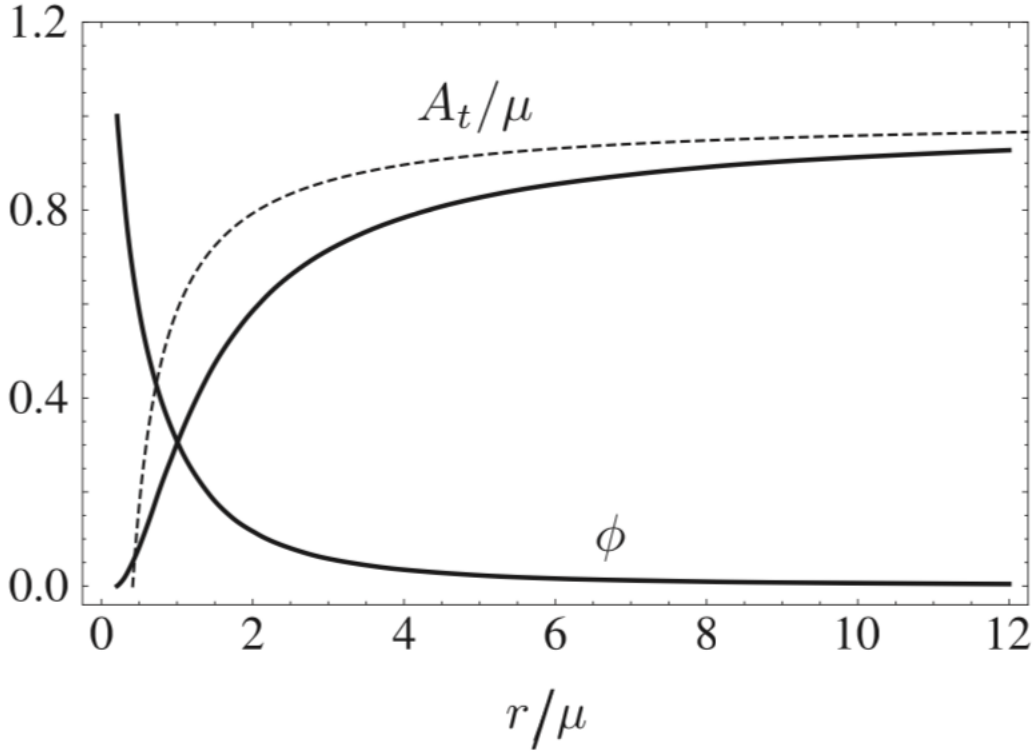

Figure 3.2: The shape of the gauge fields A_t and scalar hair Φ (denoted as ϕ in the plot) along the holographic direction $r = \frac{L^2}{z}$ for the massive complex scalar field with mass-squared $m^2L^2 = -2$ and charge $q = 3$ in the standard normalization for $T = 0.157$. Here every dimensional quantity is in the units of μ. Dashed line represent the solution without hair at the same temperature. The figure is taken from [36]

following fashion:[2]

$$\Phi = Jz^{\delta_1} + C \langle \mathcal{O} \rangle z^{\delta_2} + \ldots, \tag{3.12}$$

where C is some constant. In the back-reacted hair solutions, we have the freedom to set $J = 0$, but if we do that, we still observe that the VEV $\langle \mathcal{O} \rangle$ is nonvanishing. In the field theory side, the order parameter gains a VEV without a presence of any source, which means that the symmetry of $U(1)$ is broken spontaneously, i.e superconductivity is formed.

We should note that since the geometry of the deep IR is altered below some critical temperature T_c, the field theory flowed to a new IR, where superconductivity is present as we argued. It

[2] We will not discuss normalizable vs. non-normalizable solutions here. By our choice in the later chapters, every solution we consider will be normalizable.

is argued that this transition is similar to the formation of superconductivity in the strange metals. For a comparison of these phenomenons look [36].

Also we swept the fact that cuprates are d-wave superconductors rather than s-wave under the rug in the discussion above [31]. It turns out that it is possible to model these systems via holography and get the relevant physics, however the complication associated with it in the gravitational side (i.e having another spin-2 field besides graviton and making it massive) makes them hard to deal with compared to the s-wave models [8]. So often times s-wave models give us general features without too much complication.

Lastly, note that this model of superconductivity is *global*, in the sense that superconductivity forms on the boundary has the same VEV at every point on the boundary, as suggested by the shape in figure (3.2). Related to that, its critical temperature increases linearly with the chemical potential, $T_c \sim \mu$. However, in the real-world strange metals, this model might be an oversimplification and it is easy to imagine that the superconductivity is localized to some region on boundary because of some impurity of dopants or any other experimental reason. So it might be a good idea to model these system holographically as well then. We will turn this question in chapter (5).

3.4 Charged Defects

In the last section of this chapter, we change gears and discuss the models of charged defects in the holographic context discussed in [9, 24, 27]. Our aim is to summarize important points and describe how to combine the physics of superconductivity on top of charged defects in strange metals at finite temperature.

So, start with defining what we mean by a charged defect. An *electrically charged defect* is a configuration of the chemical potential at the boundary that is spherically symmetric and dies off far away from the symmetry axis [24]

$$\mu = \mu(r) \quad \text{and} \quad \lim_{r\to\infty} \mu(r) = 0. \tag{3.13}$$

Here, and henceforth, r will denote the radial coordinate and φ will denote the angular coordinate in the boundary of AdS.[3]

From now on we will focus on the case $d = 2$. That means we are considering 2+1 dimensional CFT and naturally its dual becomes AdS_4. This choice is motivated by the fact that in cuprates or related materials are essentially quasi-two-dimensional when their superconductivity properties are considered [31].

Note that we have broken one of the translational symmetries in the system by introducing a spherically symmetric modulation for the chemical potential. Therefore in AdS dual, we will only have two Killing vectors ∂_t and ∂_φ corresponding to the time-invariance and cylindrical symmetry. So the solutions we are looking for are going to be static, axisymmetric asymptotically AdS_4 spacetimes, possibly with a scalar hair and nonvanishing gauge field. Killing vectors of this configuration shows that our problem is cohomogenity-2, meaning that the solutions we are looking for is going to be effectively two dimensional, depending on the holographic and radial directions, z and r.

As we will see explicitly, this complication results in 7 coupled, nonlinear, partial differential equations we need to consider on a rectangular domain, which poses a great technical challenge to solve. We will describe the numerical methods we will employ in the chapter (4) below in more detail.

It is easy to imagine that adding such a chemical potential will in general makes the CFT flow to different low-energy. In general, this is true, however it is not complete. We should determine the RG flow the charged defects induces to decide this, which we will do by counting dimensions, following [24]. In order to do this, observe that the chemical potential should have mass dimension 1, by the fact that the action is dimensionless and the charge density has mass dimension 3 considering the coupling (2.27). That means, given the large r behavior for charge defect is

$$\mu(r) \sim \frac{\alpha}{r^n}, \tag{3.14}$$

we see the mass dimension of α is $1 - n$. From this we immediately conclude for $n < 1$ the defect

[3] Note that some authors use r for the holographic direction. For us z is always the holographic direction and r is always the radial direction in the boundary.

is relevant, for $n = 1$ it is marginal and $n > 1$ it is irrelevant deformation. Note that this matches our intuition, sufficiently localized defects do not alter the low energy physics too much and can be investigated perturbatively.

The relevant deformations are going to change the low-energy physics significantly by driving the field theory to a different IR fixed points. In practice, we discovered that it is hard to construct these solutions numerically since IR becomes singular and those solutions are numerically unstable. So in this study, we won't consider relevant defects.

Therefore, we will mostly consider irrelevant defects for which IR is not significantly altered and generally numerically stable.[4] These defects are numerically easy to work with because implementing the boundary condition at the horizon is a trivial pursuit, for which we will just demand regularity.

In the literature, the solutions at zero [24] and finite temperature [27] for irrelevant and marginal defects (without scalar hair) are discovered numerically. These systems are interesting in various ways. For example, at the zero temperature it is found that the solutions of these systems include a spherical *hovering black hole* for which entropy scales the same way for every type of defect [24] . We postpone our discussion of hovering black hole for later in chapter (6).

At finite temperature, with the presence of the charged defect, it has been found that the horizon of the black hole is highly deformed and looks like a "mushroom" when it is isometrically embedded to $\mathbb{R}^2$ [27]. The authors therefore called this solution *black mushroom* and we will adopt this terminology as well. Moreover, it has been found that these solution might violate the cosmic censorship in the same study [27]. Later, these results discussed more in depth with the consideration of the scalar field at the zero temperature and its relation to the weak gravity conjecture [9].[5]

As one can sense, in these studies the focus was mostly on the gravitational dynamics of the system and occasional comments on the corresponding physics at the boundary. In this study, we

[4] We might consider marginal defects as well, but we opt not to do so since they don't give any new physics.
[5] This system can actually be considered the zero temperature version of the system we are going to study here.

will reverse this direction and ask the question what these systems mean from the boundary point of view, especially what it implies for condensed matter physics of impurities and superconductivity it forms on top of them at finite temperature, with the occasional comments on the gravitational dynamics.

Chapter 4

Numerical Methods

In this chapter, we will briefly go over the numerical techniques and tricks we used to solve the differential equations we encountered during this study. As we noted in the previous chapter, we will deal with nonlinear, coupled, partial differential equations (PDEs) and occasionally their linearized versions. We will begin with describing how we discretize our differential equations to program them into a linear solver, namely pseudo-spectral collocation on a Chebyshev grid. Then we will describe the Newton-Raphson algorithm and how we implemented it to solve the nonlinear equations and generalized eigenvalue problems for our linear equations. Lastly, we will nonrigorously touch upon the Einstein-DeTurck trick which allowed us to do all of this. We refer reader to [2, 12, 21, 33] for deeper analysis.

4.1 Pseudo-Spectral Collocation on Chebyshev Grid

Before we can program any differential equation into a computer, we need to choose a suitable grid with N_i points in the ith direction to turn the set of n differential equation equations into $\mathcal{N} \times \mathcal{N}$ matrix equations, where $\mathcal{N} = n \prod_i N_i$. The most common type of such grids are finite difference grids, where grid points are equidistant. However, as it is somewhat common in the applied holography literature, we choose our grid to be *Chebyshev grid* or *Chebyshev-Gauss-Lobatto grid* between 0 and 1. It is the set of N_i points in the ith direction [12]

$$CG_i = \left\{ \frac{1}{2} - \frac{1}{2} \cos\left(\frac{j\pi}{N_i}\right) : j = 0, 1, \ldots, N_i \right\}. \tag{4.1}$$

Observe that the grid points are not equidistant but collected near the edges because of cosine. Discretizing the equations on this grid is called *pseudo-spectral collocation on Chebyshev grid*.

One of the significant advantages of using Chebyshev grids is the fact that if the functions are smooth and remain finite (which is always true in numerics), we get an exponential convergence with the increasing grid number N_i [12], which we showed this is the case for our code in the appendix A for our system of equations. However, these grids also result in poorly-conditioned dense matrices which should be dealt with somehow. In our study, we discovered that this problem can be easily controlled by normalizing diagonal entries of resulting $\mathcal{N} \times \mathcal{N}$ matrix to 1.

It is a trivial exercise to derive the derivative operator on these grids. It is given by [12]

$$D_{ii} = \sum_{i \neq j} \frac{1}{x_i - x_j}, \tag{4.2}$$

$$D_{ij} = \frac{a_i}{a_j(x_i - x_j)} \quad \text{where} \quad a_i = \prod_{i \neq j} (x_i - xj). \tag{4.3}$$

and higher order derivatives can be calculated by multiplying this matrix by that derivative's order, $D^{(n)} \approx D^n$.

Lastly, as we said before, our problems are cohomogenity-2, which means they are effectively 2 dimensional, so as a result we have to use product of two grids, $\mathrm{CG}_1 \times \mathrm{CG}_2$. But we need to somehow create a single grid from a given product $\mathrm{CG}_1 \times \mathrm{CG}_2$ to get a proper matrix equation. This can be easily implemented by *co-lexicographic ordering*, which orders the elements of the grids as follows [2]:

$$\begin{bmatrix} a_{11} & a_{12} & \cdots \\ \vdots & \ddots & \\ a_{N_1 1} & & a_{N_1 N_2} \end{bmatrix} \rightarrow \begin{bmatrix} a_{11} \\ \vdots \\ a_{1N_2} \\ a_{21} \\ \vdots \\ a_{N_1 N_2} \end{bmatrix}, \tag{4.4}$$

where a_{ij} represents the value of the function associated with the ith point in the grid CG_1 and the jth point in the grid CG_2.

Additionally, with this choice of ordering, the partial derivative operators are given by the Kronecker product of the derivative operator in single grid with the identity operator in the other one. In other words, if $\mathbb{I}_i$ denotes the identity operator associated with the grid CG_i, the partial derivative operators that acts on the co-lexicographically ordered grid is given by [2]

$$\partial_1 = \mathbb{I}_1 \otimes D_2 \quad \text{and} \quad \partial_2 = D_1 \otimes \mathbb{I}_2, \tag{4.5}$$

where D_i represent the derivative operator on the grid CG_i and ∂_i is the partial derivative in the combined grid in the direction of CG_i. We wrote an automatic routine to implement this ordering in our code.

4.2 Newton-Raphson Algorithm

Now we will discuss the Newton-Raphson (NR) algorithm in the context of solving differential equations formally. Assume that we have a set of N partial differential equations in M dimensions (collectively shown as x) and K functions (collectively shown as f). Then this collection of differential equations can be written in the following form:[1]

$$\mathcal{F}_i = \mathcal{F}_i[x, f, \partial f]. \tag{4.6}$$

Written in this form we can view the set of PDEs as a functionals of f. Then by Taylor expanding around some set of functions, say $f^{(0)}$, we get formally

$$\mathcal{F}_i = \mathcal{F}_i^{(0)} + \left(\frac{\delta \mathcal{F}_i}{\delta f_j}\right)^{(0)} \delta f_j + \dots. \tag{4.7}$$

Here the superscript (0) indicates the functionals are evaluated at the set of functions $f^{(0)}$ and $\delta f_j = f_j - f_j^{(0)}$. Also note that the functional derivative basically indicates the linearization of PDEs around the background $f^{(0)}$, which we can do very easily by varying functions in PDEs around $f^{(0)}$ and set the coefficient of variation to zero.

[1] We assumed that the boundary conditions, if there are any, are encoded in the functional $\mathcal{F}_i$.

Observe that if $f^{(0)}$ is sufficiently close to the solution we are looking for we can solve the equation

$$-\mathcal{F}_i^{(0)} = \left(\frac{\delta \mathcal{F}_i}{\delta f_j}\right)^{(0)} \delta f_j, \tag{4.8}$$

for δf_j and get the solution for $\mathcal{F}$ with $f = f^{(0)} + \delta f$. This is the main idea behind the NR algorithm. Of course, when we encode these differential equations into a computer, the analog of the equation (4.8) becomes a finite matrix equation and it reduces to a linear algebra problem.

Hence we can summarize the NR algorithm as follows [12]:

(1) Start with choosing a suitable *seed*. In the example above this is the set of functions $f^{(0)}$ that are sufficiently close to the solution. Often times this is the hardest step in the NR algorithm, however for our problem we will always have a known solution that is continuously connected to the solution that we are looking with a parameter. This will guarantee that we can reach the solution we are looking for by taking little steps in the parameter space.

(2) Solve the discretized analog of the equation (4.8). In the example above this is equivalent to solving for δf. This is going to be the most computationally expensive part of the algorithm since the matrix equation we are solving is poorly-conditioned and dense. However, as we mentioned, this won't cause too much problem in the regime we are interested in. In order to solve this equation, we will use `LinearSolve` which is built-in function in `Mathematica`, which implements usual LU decomposition.

(3) Obtain the improved solution by adding the solution to the discretized analog of the equation (4.8) to our initial seed. If the desired convergence is reached, stop and take this to be the solution. Otherwise, make this improved solution to be the new seed and start the process again until the desired convergence is reached.

Lastly, we can quickly estimate the error of the Newton-Raphson algorithm in each iteration. Define the set of solution to be $f^{(s)}$ for the functionals $\mathcal{F}$, and let the error functions as $\epsilon^{(n)} =$

$f^{(s)} - f^{(n)}$ at the given step where the set $f^{(n)}$ denotes the values of the functions at the nth iteration. Now observe, with the suppressed indices,

$$
\begin{aligned}
&0 = \mathcal{F}[f^{(s)}] = \mathcal{F}[f^{(n)} + \epsilon^{(n)}] = \mathcal{F}[f^{(n)}] + \epsilon^{(n)} \frac{\delta \mathcal{F}}{\delta f} + \frac{1}{2}(\epsilon^{n})^2 \frac{\delta^2 \mathcal{F}}{\delta f^2} + \dots \\
&\implies -\mathcal{F}[f^{(n)}] \left(\frac{\delta \mathcal{F}}{\delta f}\right)^{-1} = \epsilon^{(n)} + \frac{1}{2}(\epsilon^{(n)})^2 \frac{\delta^2 \mathcal{F}}{\delta f^2} \left(\frac{\delta \mathcal{F}}{\delta f}\right)^{-1} \\
&\implies \epsilon^{(n+1)} = f^{(s)} - f^{(n+1)} = f^{(s)} - \left(f^{(n)} - \mathcal{F}[f^{(n)}] \left(\frac{\delta \mathcal{F}}{\delta f}\right)^{-1} \right) = -\frac{1}{2}(\epsilon^{(n)})^2 \frac{\delta^2 \mathcal{F}}{\delta f^2} \left(\frac{\delta \mathcal{F}}{\delta f}\right)^{-1} \\
&\implies \epsilon^{(n+1)} \sim (\epsilon^{(n)})^2.
\end{aligned}
$$

This shows that the NR algorithm is quadratically convergent. During our numerical calculations, this was a useful check whether or not the NR algorithm is working properly. We saw that it was following this pattern indeed.

4.3 Generalized Eigenvalue Problems

Some of the differential equations we encountered during this study were linear and they contained some parameter λ which we would like to solve for. In these cases our differential equations take the following form:

$$\left(\mathcal{D}_0 + \lambda \mathcal{D}_1 + \lambda^2 \mathcal{D}_2\right) f = 0. \tag{4.9}$$

Like above, f denotes the set of functions, and $\mathcal{D}_i$ for $i = 1, 2, 3$ are some operators that act on this set of functions. Note that we can put this equation into the following form:

$$\left(\begin{bmatrix} \mathcal{D}_1 & \mathcal{D}_0 \\ 1 & 0 \end{bmatrix} - \lambda \begin{bmatrix} -\mathcal{D}_2 & 0 \\ 0 & 1 \end{bmatrix} \right) \begin{bmatrix} \lambda f \\ f \end{bmatrix} = 0. \tag{4.10}$$

After discretizing functions and operators $\mathcal{D}_i$ properly, we see that this equation becomes a generalized eigenvalue problem in λ, which is easy to solve using built-in `EigenSystem` function in `Mathematica`. We explicitly checked that the upper half of the elements are proportional to the lower half and see that was indeed the case.

Lastly, we should note that for both $\frac{\delta \mathcal{F}}{\delta f}$ and operators $\mathcal{D}_i$, we write them in the following fashion in the expansion of the derivative operators:

$$\frac{\delta \mathcal{F}}{\delta f} \quad \text{or} \quad \mathcal{D}_i = \sum_{i\,n} c_i^{(n)} \partial_i^n, \tag{4.11}$$

and only calculated the coefficients $c_i^{(n)}$. Here ∂_i are the differential operator for partial derivatives on the combined grid we introduced in the previous section. The reason why we do that was to save the memory.

4.4 Einstein-DeTurck Trick

So far, we haven't discussed the existence of the solutions that we are looking for the case of nonlinear coupled PDEs. One can imagine that they might not even exist, and all the things might be for naught. However, this turns out not to be the case if we implement the *Einstein-DeTurck trick* that will render our problem into a well-posed boundary value problem [21].

As we will see in the next chapter, we are going to get a boundary value problem for a system of PDEs in two dimension. However, the PDEs we get would be a mix of elliptic-hyperbolic PDEs, since we are going to look for static solutions of general relativity [12]. So, the boundary value problem, as itself, is not well-defined.

However, we can render the system to be an elliptic set of equations and obtain a well-posed boundary value problem. This is done with choosing a *reference metric* $\bar{g}$ which has the same boundary conditions as the metric g we are looking for and shifting the Einstein tensor in the equations of motion [21]

$$G_{\mu\nu} \to G'_{\mu\nu} = G_{\mu\nu} - \nabla_{(\mu}\xi_{\nu)}, \quad \text{for} \quad \xi^\mu = g^{\nu\lambda}\left(\Gamma^\mu_{\nu\lambda}(g) - \Gamma^\mu_{\nu\lambda}(\bar{g})\right), \tag{4.12}$$

where $\Gamma^\mu_{\nu\lambda}(g)$ denotes the Levi-Civita connection for the metric g as usual.

It has been proven [21] that this renders a system of equations into elliptic as we desired, so we get a well-posed boundary value problem. We won't repeat the proof here, since it is out of the scope of this thesis, but we should note that it achieves that by essentially adding a kinetic term to non-physical degrees of freedom of the metric and making the gauge fixing dynamical.

Then, it is clear that the solution exists for the metric and matter fields using the equations with the shifted $G'_{\mu\nu}$. In order to get a solution for the original equations with unshifted $G_{\mu\nu}$, however, we must guarantee that $\xi = 0$ at the end. But how can we do that? Namely how can we make sure that we don't have any solutions with $\xi \neq 0$? These type of solutions are called *Ricci solitons*, which is shown to not exist for gravity without matter fields [21]. On the other hand, for our case with matter fields, there are no proofs that guarantee that such solutions do not exist.

However, since we are considering elliptic boundary value problems, we know that the solutions we find must be locally unique [12], which means that our desired solutions with $\xi = 0$ cannot be arbitrarily close to the Ricci solitons. Therefore, in numerical practice, by carefully checking the condition $\mathrm{Max}(\xi) = 0$, it is possible to obtain the solutions of the original equations.[2] However, we find that even though ξ becomes large, the solutions we find remain robust, which shows that it doesn't create a huge problem in terms of convergence.

---

[2] For its descent with increasing grid size, look appendix A.

Chapter 5

Local Holographic Superconductors

In this chapter, we explain our construction of *local* versions of holographic superconductors at finite temperature along with the physics they contain both from boundary and bulk point of views. First, we consider linear perturbations of the charged massive scalar field on top of the charged defect solutions at finite temperatures. We start by investigating the effective mass of the scalar field, as well as how it results in instabilities with its zero modes numerically. We show that zero modes of the linear perturbations of the scalar field exist for low enough temperatures or high enough charges. We see that these modes mark the boundary between stable and unstable regimes by explicitly showing the progression of the lowest-lying zero mode from the lower half frequency plane to the upper half frequency plane.

After we solved for linear perturbations, we construct the fully back-reacted solution which is the end point of the scalar instability we mentioned above. We call this solution *hairy black mushroom*, since it basically develops a hair on top of the black mushroom solution in [27]. We will show that superconductivity on the boundary is localized around the charged defect as our intuition suggests. We explain the similarities and differences between the previously constructed global holographic superconductors and find that there are novel effects that have no analog in the global case, such as in what regime superconductivity is more robust and how the critical temperature changes with increasing amplitude of the defect.

Moreover, we will check the scaling behavior and confirm that the transition to local holographic superconductivity is a mean-field type, like in the global case, but with different coefficients on each point on the boundary. Lastly we will briefly look at the free energy and explicitly check that the superconducting phase we constructed is dominant in the grand canonical ensemble against the normal phase.

5.1 Setup

Our setup will be like in chapter (3), but with a slight difference in the normalization of fields to make the numerics simpler. Our action is given by

$$S = \frac{1}{16\pi G} \int \mathrm{d}^4x\sqrt{-g}\left[R + \frac{6}{L^2} - F^{\mu\nu}F_{\mu\nu} - 4\left|\partial_\mu\Phi - iqA_\mu\Phi\right|^2 - 4m^2\left|\Phi\right|^2\right], \tag{5.1}$$

here L is the AdS radius, the field Φ is a massive charged complex scalar field with a mass m and charge q. The Maxwell field satisfies $F = \mathrm{d}A$ as usual. Henceforth, we will set $L = 1$ without loss of generality, which we can restore by dimensional analysis later on if we want.[1] The resulting equations of motion are

$$G_{\mu\nu} = R_{\mu\nu} + 3g_{\mu\nu} = 2(T^{EM}_{\mu\nu} + T^{\Phi}_{\mu\nu}), \tag{5.2}$$

$$\nabla_\mu F^{\mu}_{\ \nu} = J^{\Phi}_{\nu}, \tag{5.3}$$

$$\mathcal{D}_\mu\mathcal{D}^\mu\Phi = 0, \tag{5.4}$$

where the stress-energy tensors $T^{EM}_{\mu\nu}$, $T^{\Phi}_{\mu\nu}$ for the electromagnetic and the scalar fields, the electromagnetic current J^{Φ}_{μ}, and the covariant derivative (both for coordinate and U(1) gauge transformations) $\mathcal{D}_\mu$ are given by

$$T^{EM}_{\mu\nu} = F_{\mu}^{\ \rho}F_{\nu\rho} - \frac{1}{4}g_{\mu\nu}F^{\sigma\lambda}F_{\sigma\lambda} \tag{5.5}$$

$$T^{\Phi}_{\mu\nu} = (\mathcal{D}_\mu\Phi)(\mathcal{D}_\nu\Phi)^\dagger + (\mathcal{D}_\mu\Phi)^\dagger(\mathcal{D}_\nu\Phi) + g_{\mu\nu}m^2\left|\Phi\right|^2, \tag{5.6}$$

$$J^{\Phi}_{\mu} = iq\left((\mathcal{D}_\mu\Phi)\Phi^\dagger - (\mathcal{D}_\mu\Phi)^\dagger\Phi\right), \tag{5.7}$$

$$\mathcal{D}_\mu = \nabla_\mu - iqA_\mu. \tag{5.8}$$

[1] Also, by our choice of gauge couplings, all of the formulas will be independent of Newton's Constant. So we will not set it to 1.

where ∇ is the covariant derivative just for the coordinate transformation. Observe that we can make a global U(1) transformation on the scalar field $\Phi \to e^{i\chi}\Phi$, for constant χ, and the field equation would remain invariant. So, without loss of generality, we can take the field Φ to be real, $\Phi \in \mathbb{R}$, which we will do below. Also, this means the sign of Φ does not matter as well, we can always change the sign by taking $\chi = \pi$ above.

Since we are seeking solutions that asymptote to AdS_4 and the asymptotic boundary of AdS is timelike [1], we are free to specify the metric and the gauge field on the boundary. We choose them to be

$$\mathrm{d}s^2|_\partial = -\mathrm{d}t^2 + \mathrm{d}r^2 + r^2\mathrm{d}\varphi^2, \tag{5.9}$$

$$A|_\partial = \mu(r)\mathrm{d}t = \alpha\zeta(r)\mathrm{d}t, \tag{5.10}$$

in order to have a radially decreasing chemical potential on the flat boundary, as we mentioned before. Here (r, φ) are the usual polar coordinates on the flat boundary. We have taken the dimensional amplitude α out of the chemical potential $\mu(r)$ and we call the remaining part $\zeta(r)$ the *defect profile*, which is just a chemical potential for which the amplitude is normalized to unity. Some of the examples of (irrelevant) profiles we used in this thesis are shown in figure (5.1).

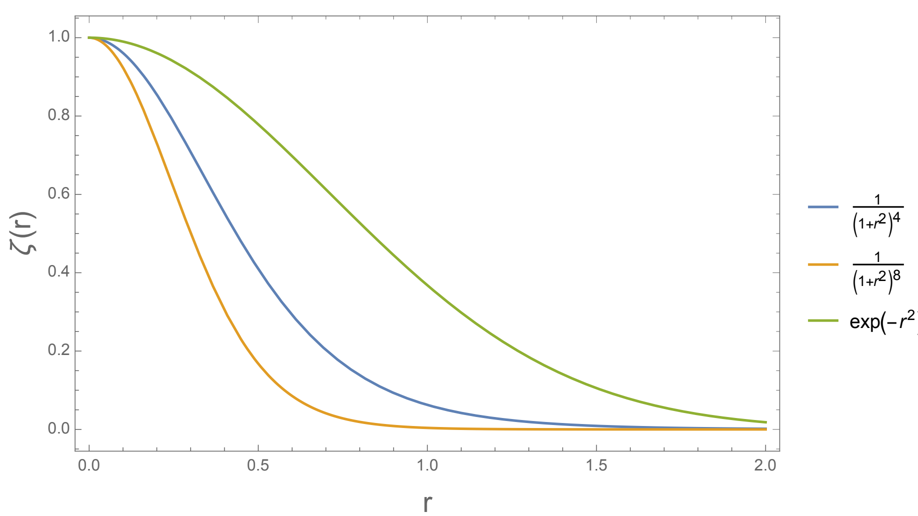

Figure 5.1: Profiles we focused on in this thesis. Note that they are spherically symmetric and irrelevantly dies off as $r \to \infty$ in the sense of chapter (3).

For numerical simplicity, rather than working in the coordinates (t, z, r, ϕ), we make the following change of coordinates

$$z = \frac{1-y}{z_+}, \qquad r = \frac{x\sqrt{2-x^2}}{1-x^2}. \tag{5.11}$$

Here, z_+ would be the distance of the horizon given in the AdS-Schwarzschild metric (2.3) which we will use as the reference metric in the Einstein-DeTurck trick (4.4).

Note that, the horizon is mapped to $y = 0$ while the asymptotic boundary is mapped to $y = 1$ in these coordinates. On the other hand, the radial coordinates mapped between 0 and 1: The symmetry axis of spacetime is mapped to $x = 0$ and the asymptotic radial boundary is mapped to $x = 1$. Basically, this squishes the conformal plane determined by z and r to a rectangular region $[0, 1] \times [0, 1]$, for which we will put the discretized grid on, defined in chapter (4).

We write (2.3) again, but in the coordinates (5.11) for reference,

$$\mathrm{d}s^2 = \frac{1}{(1-y)^2}\left(-z_+^2 g(y)\mathrm{d}t^2 + \frac{\mathrm{d}y^2}{g(y)} + \frac{4z_+^2\mathrm{d}r^2}{(2-x^2)(1-x^2)^4} + \frac{z_+^2 x^2(2-x^2)}{(1-x^2)^2}\mathrm{d}\varphi^2\right) \tag{5.12}$$

where $g(y) = y^3 - 3y^2 + 3y$ is the emblackening factor in these coordinates. Observe that it vanishes for $y = 0$, where the horizon resides as it should be.

5.1.1 Black Mushroom

We will first solve for the case without a scalar field to investigate the scalar perturbation on top of the charged defect. In [27], the authors have solved the equations of motion numerically for the static case with a vanishing scalar field and nontrivial radially decreasing chemical potential for the following metric and gauge field ansatz already,

$$\begin{aligned}\mathrm{d}s^2 = \frac{1}{(1-y)^2}\Bigg(& -z_+^2 g(y)Q_1(x,y)\mathrm{d}t^2 + \frac{Q_2(x,y)}{g(y)}\left[\mathrm{d}y + \frac{yQ_3(x,y)}{(1-x^2)^2}\mathrm{d}x\right]^2 \\ & + \frac{4z_+^2 Q_4(x,y)}{(2-x^2)(1-x^2)^4}\mathrm{d}x^2 + \frac{z_+^2 x^2(2-x^2)Q_5(x,y)}{(1-x^2)^2}\mathrm{d}\phi^2\Bigg),\end{aligned} \tag{5.13}$$

$$A = yQ_6(x,y)\mathrm{d}t. \tag{5.14}$$

Here $Q_i(x, y)$ for $i = 1, \ldots, 6$ are the metric functions that have been solved numerically. The sample plots of these functions for the profile $\zeta(r) = (1 + r^2)^{-4}$ we produced with our code again are shown in figure (5.2) and its convergence analysis is given in the appendix A.

Note that temperature of this solution is given by

$$T = \frac{3z_+}{4\pi} \tag{5.15}$$

as we can easily find by demanding regularity on the horizon as we mentioned before, which is in fact assumed as boundary conditions. For more details regarding the numerical implementation, boundary conditions, and its physics, see [27]. However, the authors there didn't give induced charge density at finite temperature, so we are going to spend some time on them because we will need them when we are describing our system of interest, namely local holographic superconductors, later on.

The charge densities induced on the boundary by such electrically charged defect profiles are shown in figure (5.3), which we find them using AdS/CFT dictionary. As we can see, such chemical potentials localize charges around the origin. But since the defect collects too much charge it screens itself and results in oscillating behavior. This is typical to the behavior of impurities in the plasma or metal mediums and in some sense similar to Friedel oscillations in Fermi liquids. For holographic investigation of this effect in the linear response, see [5].

As can be seen from the figures, as we increase the chemical potential, it induces more charge, which is somewhat expected. Moreover, as temperature increases, there is more induced charge. Lastly, by making the defect more local, we make the charge density at the boundary more local. Again, these fit our intuition as well.

We are going to use this finite temperature solution (5.13) as our background to investigate the behavior of the scalar field, and later on, using zero modes of the scalar field perturbations as a seed for the Newton-Raphson algorithm to find the hairy solution. Since we are going to use the metric (5.13) as our seed, temperature would still be given by (5.15) for our new solutions.

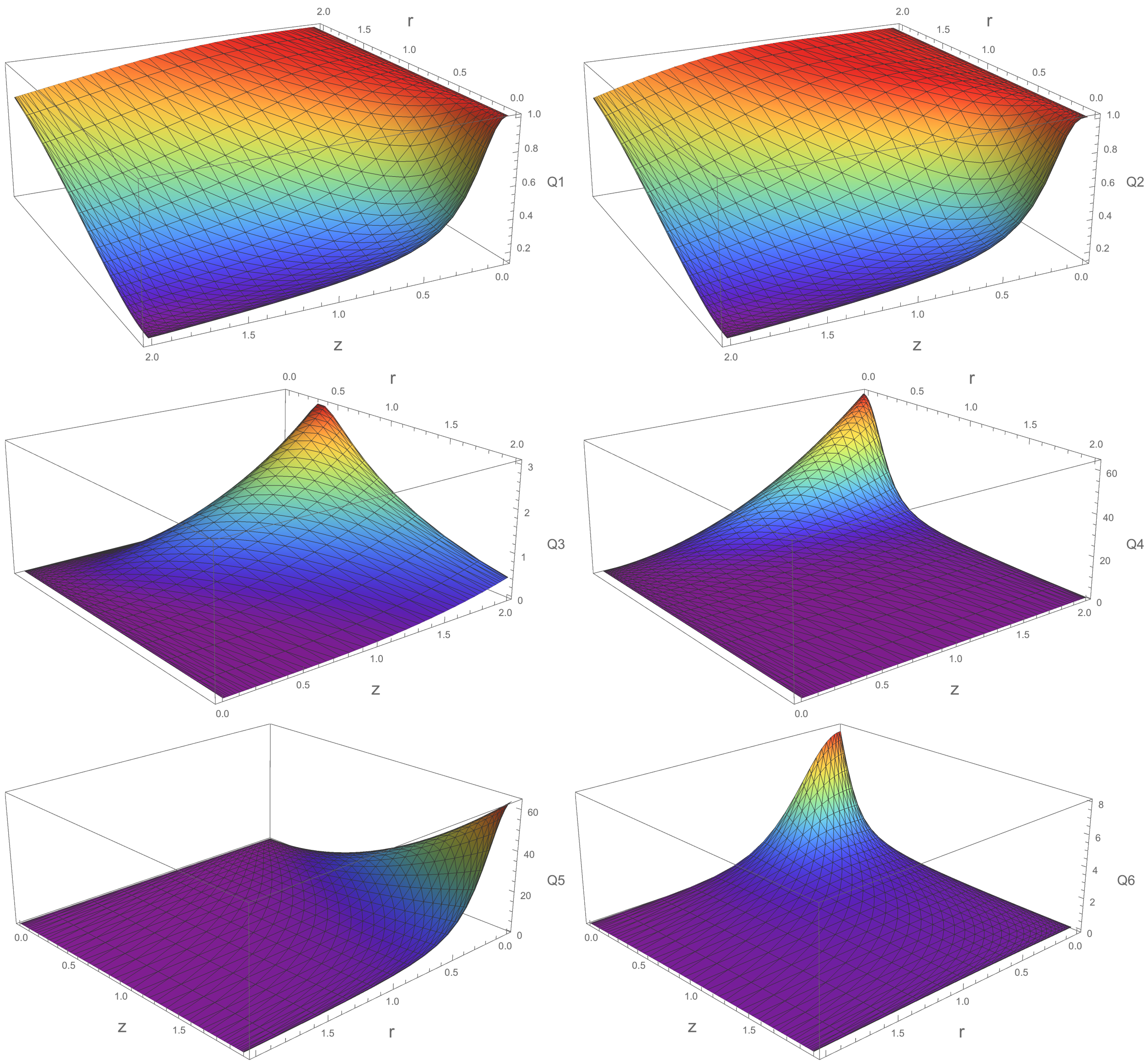

Figure 5.2: The functions $Q_i, i = 1, \ldots, 6$ for $T = 0.119$ and $\alpha = 8$ in the conformal plane are shown above. As we can see they are nontrivial.

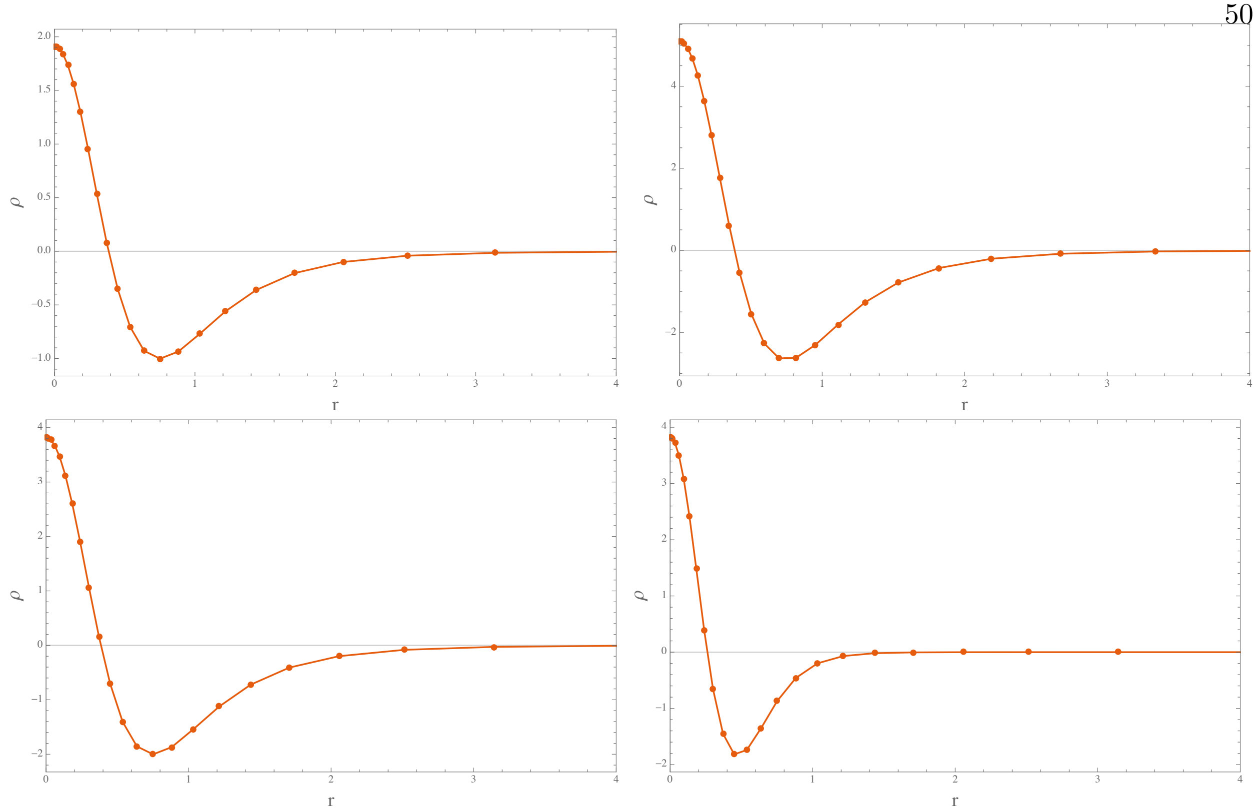

Figure 5.3: Sample charge densities ρ induced by the defect profile $\zeta(r) = (1+r^2)^{-4}$ for $T = 0.119, \alpha = 3$ (upper-left), $T = 0.119, \alpha = 8$ (upper-right), and $T = 0.239, \alpha = 3$ (lower-left). Lastly we have the charge density induced by the defect for $\zeta(r) = (1+r^2)^{-8}$ for $T = 0.119, \alpha = 3$ (lower-right).

5.2 Scalar Field Perturbations

Now we will consider the linear perturbations of the scalar field in the background (5.13) of the type $\Phi = \Phi(x,y)e^{-i\omega t}$ at finite temperature. We will assume that there is no angular dependence on the scalar field Φ, which will result in spherically symmetric superconductivity at the end. Also we will consider the case where the perturbations of the scalar field have $e^{-i\omega t}$ dependence in time since the solution is static (i.e. translationally symmetric in time so it is sufficient to consider only one of its Fourier components in its decomposition which we can add them later on if we want to add the time dependence). Below, we will first specialize in the case of $\omega = 0$, which is known as the *zero mode* and in the next subsection we will investigate its progression in the complex ω plane.

Henceforth, we will work with a scalar field with a mass $m^2 = -2$, corresponding to the scalar order parameter with the conformal dimension $\Delta = 2$ on the boundary by (2.1) and the solutions we will choose are going to be normalizable [1]. These choices are motivated by the fact that exponents of the asymptotic expansion of the scalar field near the boundary will be non-negative integers with such choices, which will improve the convergence and numerics. In theory, any other choice of m and/or non-normalizablility shouldn't change the results below.

5.2.1 Zero Modes

Note that for the zero modes of the scalar field perturbations of the type $\Phi = \Phi(x, y)$, the scalar equation of motion (5.4) simplifies to

$$\nabla^2\Phi = (m^2 + q^2A^2)\Phi, \tag{5.16}$$

where ∇^2 is the Laplacian in the black mushroom background (5.13). Observe that the right hand side defines the effective mass of the scalar field in the background (5.13). This is given explicitly as

$$m^2_{eff}(z, r) = m^2 + q^2A^2(z, r) = m^2 - \frac{q^2(y-1)^2y^2Q_6(x, y)}{g(y)z_+^2Q_1(x, y)}. \tag{5.17}$$

Observe that it is always the case that $m^2_{eff} \leq m^2$, as we can easily see from the fact that every factor in the second term is positive. Also, observe that the effective mass depends on the radial direction in the conformal plane of AdS through the dependence of the coordinate x, unlike the AdS-RN black hole background which has no such dependence, look at the figure (5.4). This would be the main reason why we will have localized behavior for the instabilities and scalar hair below.

We want to find a solution of (5.16) for the scalar field Φ at the given temperature T. By noting that the equation (5.16) is just a quadratic eigenvalue problem in q, we can solve it using the methods described in chapter (4) to find the smallest $q = q_{min}$ such that a nontrivial solution of (5.16) exists. In order to do that we demand the following boundary condition for the perturbations,

$$\partial_x\Phi(0, y) = 0, \quad \Phi(1, y) = 0, \quad \Phi(x, y \approx 1) = \mathcal{O}(y^3), \tag{5.18}$$

and we demand regularity on the horizon by imposing the series expansion of the equation of motion

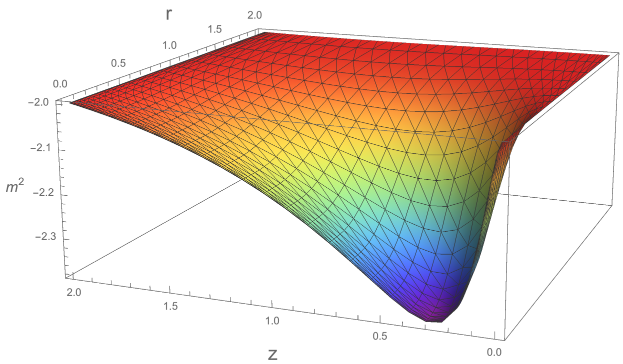

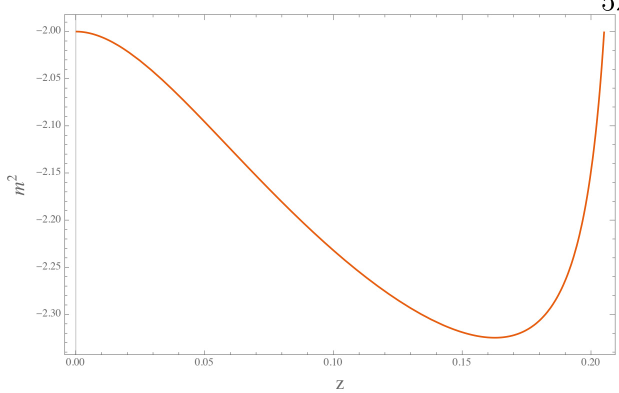

Figure 5.4: The (numerical) effective mass for the defect profile $\zeta(r) = (1 + r^2)^{-4}$ and the global (AdS-RN) case for $T = 0.119$ and $\alpha = 8$ in the conformal plane (left). The (closed-form) effective mass in the AdS-RN background at the same temperature with the uniform chemical potential $\mu = 8$ (right). In both of the graphs, the charge of the scalar field is normalized to unity, $q = 1$. As one can see, there is no radial dependence on the second plot and the position of the horizon is reversed. In theory, the shape is similar for other profiles as well.

at $y = 0$ which results in a smooth metric and fields at the horizon. Doing this was somewhat long so we didn't report it here.

Note that these choices for the boundary conditions are well-motivated. For the first condition, we want the scalar field to be smooth on the symmetry axis without any "kinks". For the second condition, we want no scalar perturbation away from the symmetry axis, since there is no charge there and fluctuations should die away in that region. For the third condition, we want the VEV of the operator that the scalar field Φ dualizes to be nonzero without a source to model superconductivity, so we demand that the leading term in the asymptotic expansion for the field Φ vanishes by AdS/CFT dictionary. Lastly, we demand regularity on the black hole horizon in order not to change the temperature of the system.

We solved the equation (5.16) with the boundary conditions (5.18) for the scalar field Φ at various temperatures T, strengths α and types of the charged defects $\zeta(r)$. From this, we deduce the dependence of the minimum charge $q = q_{min}$ to nontrivial zero mode to appear at that particular temperature and strength of the defect. Plots for these are shown below in figure (5.5).

As one can see, the minimum charge necessary for the zero mode to appear decreases as the

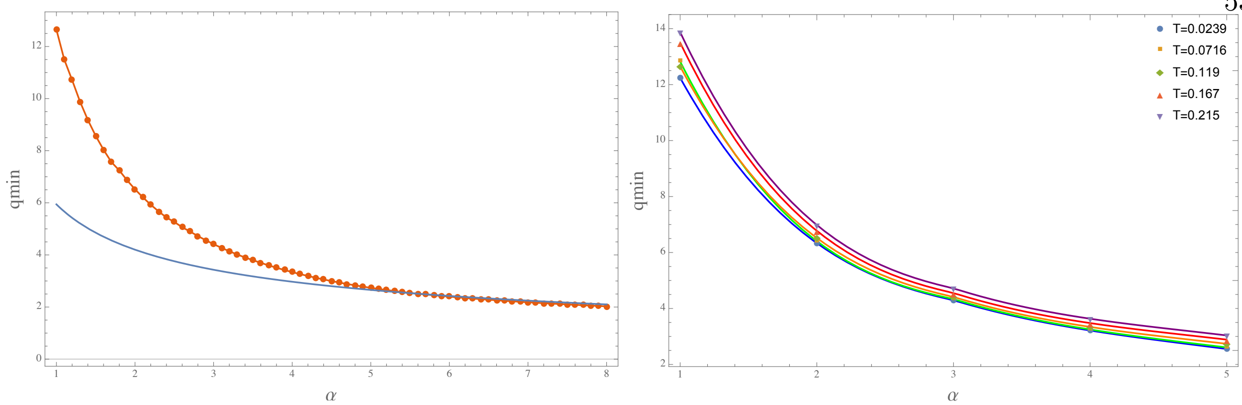

Figure 5.5: Dependence of q_{min} to the strength of the defect for the profile $\zeta(r) = (1 + r^2)^{-4}$ at temperature $T = 0.119$ with an inverse square root fit for sufficiently large α (left) and dependence of curves to different temperatures for the same defect profile (right). Note that as temperature increases the minimum charge also increases, because it becomes harder to violate the BF-like bound in such cases.

strength of the defect increases. This result makes perfect sense when we consider the effective mass (5.17) and the instability bound. As we increase the defect strength, the function $Q_6(x, y)$ increases, which makes the bound being more easily violated. Although it is hard to see in figure (5.5), the minimum charge q_{min} actually slowly descends to zero, which again makes sense by this reasoning as well.

Also, we should note that changing the defect profile doesn't alter the shape of the plot significantly, see figure (5.6). That includes the AdS-RN solution, i.e. where the chemical potential is constant on the boundary. We can see it by using dimensional analysis. In the AdS-RN solution, we can relate the critical temperature and the magnitude of the chemical potential as follows. First note that the critical temperature should be related to the charge density as $T_c \sim \rho^{1/2}$, using the residual conformal invariance in these solutions [18]. Then recalling that $\rho \sim \mu e^2$ [20] in the regime (that is $\mu \gg T$) we are interested in, we see the relation at constant critical temperature is just $e \sim \mu^{-1/2}$, which is essentially what we see in figure (5.5). So we can simply explain the effect we saw in figure (5.5) by noting that the scale related to the defect α becomes larger than the thermal scales, which effectively makes the defect look like a global chemical potential.

Because of this reasoning, we fit our result to $\alpha^{-1/2}$ for large α. As we can see from figure

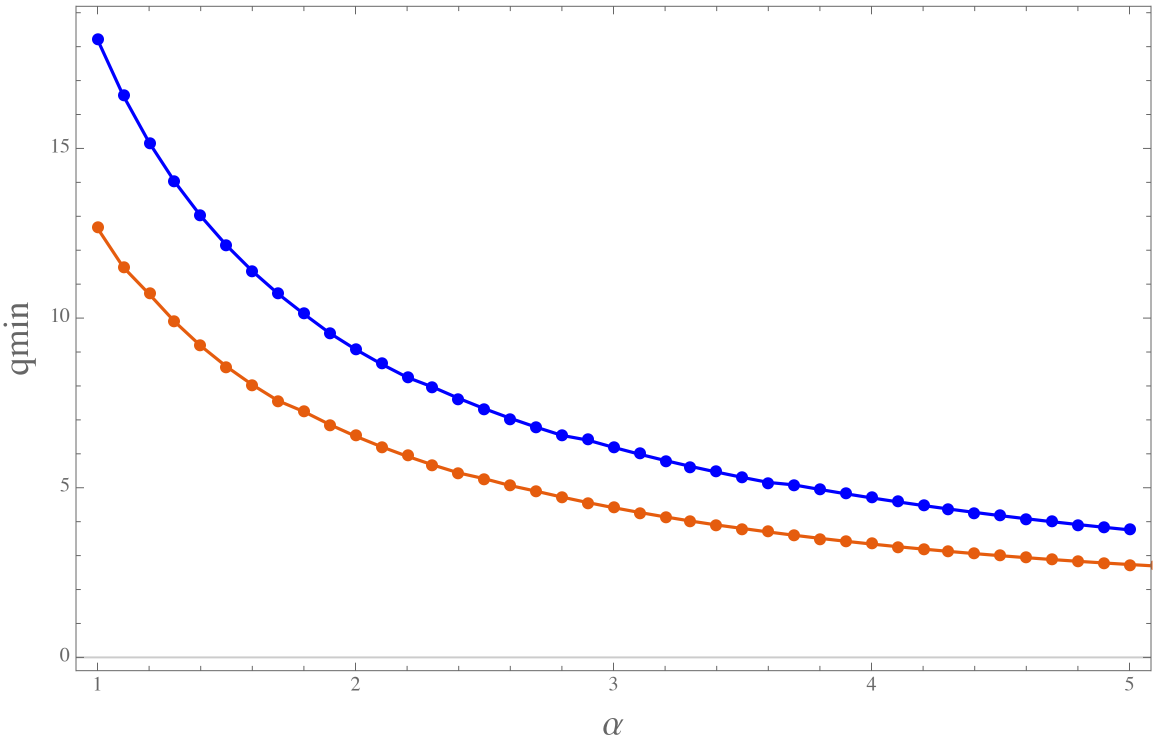

Figure 5.6: Here we plot q_{min} for two profiles $(1+r^2)^n$ at temperature $T = 0.119$, where $n = 4$ for the orange curve and $n = 8$ for the blue curve. As we can see, the only effect of making the defect more localized is to increase the charge required for the field to condense, otherwise the shape remains similar.

(5.5), the fit was successful and shows that $q_{min} \approx 5.94\alpha^{-1/2}$ for $\alpha \gg T$, which then makes us conclude that this system is similar to AdS-RN for sufficiently high enough chemical potentials and fits our intuition. Similar reasoning shows that the charge necessary for a zero mode to appear increases as temperature increases, since now it is harder to violate the instability bound. We will interpolate the dependence of the critical temperature to the strength of the defect for a fixed charge from these results later on after we build the back-reacted solution, since it deserves its own section.

Sample shapes for the the zero mode perturbations are given in figure (5.7). Observe that it indeed shows a local behavior which is somewhat expected by the spherically symmetrically modulated chemical potential and charge density above. However, what is not expected is the behavior in the holographic direction z when α is small. As we can see the perturbations are maximum in some mid-scale in z, rather than near the horizon like in the AdS-RN, for which an example is given in figure (3.2), if α is sufficiently small. However, when it gets big we see that the shape becomes similar to figure (3.2), only with somewhat expected radial modulation.

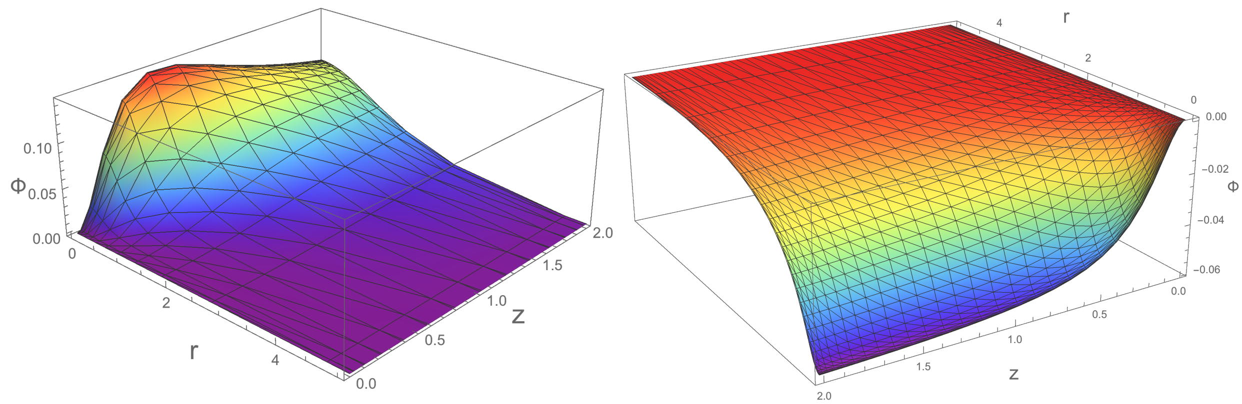

Figure 5.7: The shape of the scalar hair for the profile $(1 + r^2)^{-4}$ at temperature $T = 0.096$ and $\alpha = 3$ and $\alpha = 8$ in the probe-limit. Notice the interesting behavior for $z \approx 0.75$ for $\alpha = 3$. Also recall that these are in the linear approximation, so the size of the perturbation doesn't matter.

Since we are working in the linear regime (probe-limit) at the moment, we avoid making any interpretation of this fact, since this modulation might be removed by the gravitational back-reaction of the scalar field. However, we will observe that this is not the case below and this novel shape will stay robust. We will describe this interesting behavior after we construct the back-reacted solution.

5.2.2 Progression of Zero Modes

In the last section, we showed that zero modes of linear perturbations of the scalar field in the background of the defect exist at certain $q = q_{min}$, given temperature T, the strength and type of the defect, which indicates that the scalar perturbations with $q \geq q_{min}$ lead to instability. Now, we are going to show that such zero modes are indeed an indicator of the scalar instability, by showing the progression of the zero frequency mode of the scalar perturbation as we vary the charge q, from below q_{min} to above it, in the complex frequency plane.

We will do this by solving the equation (5.4) with the ansatz $\Phi = \Phi(x, y)e^{-i\omega t}$ using the boundary conditions (5.18) again. However, for the boundary condition at the black hole horizon, we now additionally impose infalling boundary conditions, which means the scalar field near the horizon $y \approx 0$ is given by

$$\Phi(x, y \approx 0) = y^{-\frac{i\omega}{3z_+}} \left(c_0(x) + c_1(x)y + \dots\right), \tag{5.19}$$

in order to get a proper dissipate behavior at the horizon, see [20].

In this case we will input the charge q to the equation and we are going to think the problem as a quadratic eigenvalue problem in the frequency ω instead, which we know how to solve for numerically as well. Note that this is a quadratic eigenvalue problem because the equation (5.4) is simply a second-order, linear differential equation, so we just replace $\frac{\partial}{\partial t} \to -i\omega$ by our ansatz, which results in ω^2 dependence.

If the zero modes we discovered above mark the boundary between stable and unstable modes, it must be the case that as we increase q from below q_{min} to above it, the corresponding mode should shift from the lower half-plane to the upper half-plane in the complex frequency plane. That way, we will show the existence of the scalar instability precisely, since the perturbation $\Phi \sim e^{-i\omega t} \sim e^{Im(\omega)t}$ will grow without a bound, and it will drive the system to a new solution. The progression plot for the case with the defect $\mu(r) = 3(1+r^2)^4$ is shown in figure (5.8).

As one can see, as we increase the charge q from below q_{min} to above it, the lowest lying mode moves gradually to the upper half of the frequency plane, indicating that the scalar instability and the zero mode we found in the previous subsection is indeed marking the boundary between the stable and unstable perturbations. This also indicates that there must be new solutions of (5.2), (5.3), and (5.4) at the end of these instabilities, which will discharge the black mushroom and form a scalar hair outside by the spontaneous pair production process we mentioned in section (3.3). The only difference would be the change in the region where discharging happens as evident by figure (5.7) or the effective mass m_{eff}.

This behavior happens for all of the cases we investigated in this project, so we won't repeat all of them here because it would be redundant. Similarly, we varied the critical temperature above

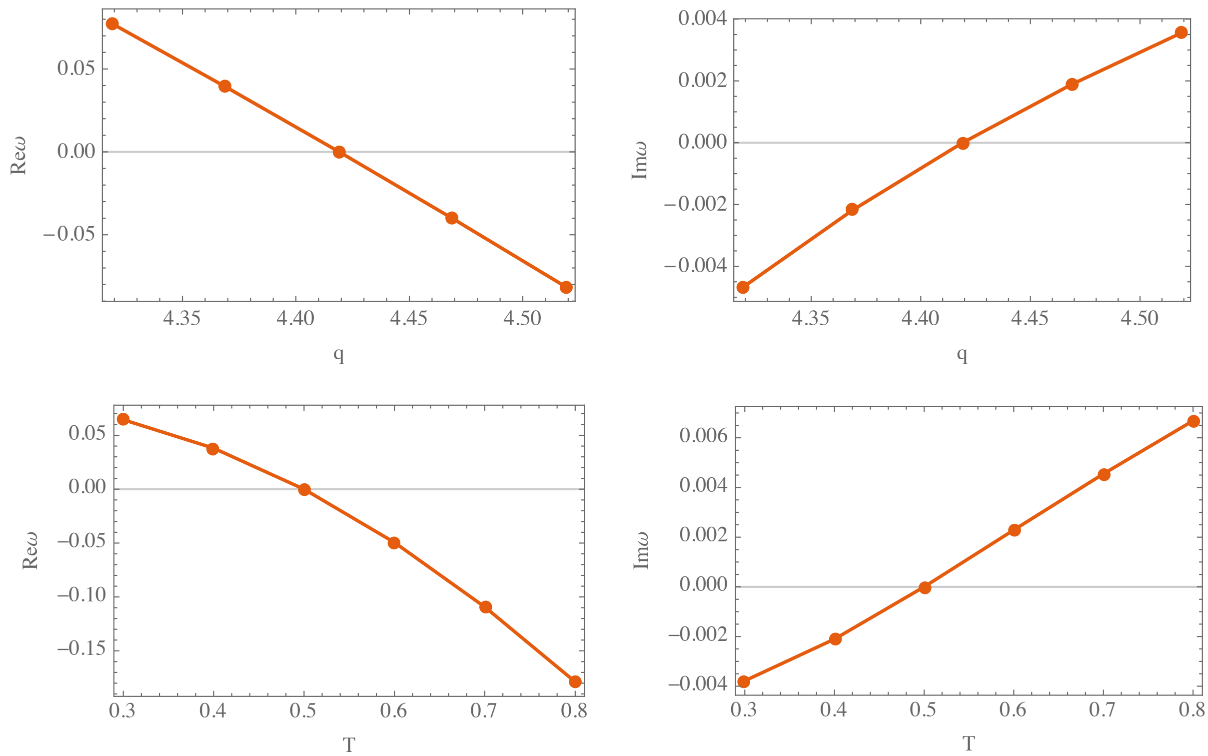

Figure 5.8: The progression of the zero mode in the complex frequency plane with charge at temperature $T = 0.119$ (top) and with temperature for $\alpha = 3$ (bottom). Here T denotes z_+. As can be easily seen, it indeed moves toward the upper half-plane for both of the cases.

and below for the lowest lying mode and saw that it also marked the instability, as can be seen in figure (5.8) as well.

Note that by the shape of the perturbation in figure (5.7), these instabilities are local in nature, they will only alter part of the spacetime close to the horizon and symmetry axis, since the perturbation localized on that area and can violate the analog of the BF bound only there. So, by this reasoning and AdS/CFT dictionary, we discover that the low-energy physics near the origin would be modified nontrivially. In the next section we will find the endpoint of these local instabilities considering their gravitational back-reaction.

5.3 Hairy Black Mushroom

In this section, we are going to numerically construct the endpoint of the local scalar instability that we discovered in the section above using the zero modes on the background of the black mushroom. Our ansatz for the solution would be

$$\begin{aligned} \mathrm{d}s^2 = \frac{1}{(1-y)^2}\Bigg(& -z_+^2 g(y) F_1(x,y)\mathrm{d}t^2 + \frac{F_2(x,y)}{g(y)}\left[\mathrm{d}y + \frac{yF_3(x,y)}{(1-x^2)^2}\right]^2 \\ & + \frac{4z_+^2 F_4(x,y)\mathrm{d}r^2}{(2-x^2)(1-x^2)^4} + \frac{z_+^2 x^2(2-x^2)F_5(x,y)}{(1-x^2)^2}\mathrm{d}\phi^2\Bigg) \end{aligned} \tag{5.20}$$

$$A = yF_6(x,y)\mathrm{d}t \tag{5.21}$$

$$\Phi = F_7(x,y). \tag{5.22}$$

Here the functions $F_i(x,y)$ for $i = 1 \ldots 7$ are assumed to be smooth. Note that the metric and the gauge field ansatz are the same as the black mushroom ansatz (5.13) and (5.14). However, we now have a nonvanishing scalar field which will produce the scalar hair in spacetime. We assume that these functions satisfy the following boundary conditions on the asymptotic boundary $y = 1$:

$$\begin{aligned} &F_1(x,1) = 1, && F_2(x,1) = 1, \\ &F_3(x,1) = 0, && F_4(x,1) = 1, \\ &F_5(x,1) = 1, && F_6(x,1) = \mu\left(\frac{x\sqrt{2-x^2}}{1-x^2}\right), \\ &F_7(x,1) = \langle\Phi\left(\frac{x\sqrt{2-x^2}}{1-x^2}\right)\rangle\, z^3 + \mathcal{O}(z^4) && \end{aligned} \tag{5.23}$$

in order to have the metric asymptote to AdS_4, A_t to the charged defect, and get the superconducting phase for which there is a nonvanishing VEV without a source turned on for the scalar field, like in the global case. Here, the function $\langle\Phi\rangle = \langle\Phi(r)\rangle$ denotes the radially dependent VEV of the scalar field on the boundary, which we used the same symbol Φ to denote the order parameter in CFT and its dual field in AdS.

Similarly, for the radial infinity $x = 1$, we assume the following boundary conditions:

$$
\begin{aligned}
&F_1(1,y) = 1, && F_2(1,y) = 1, \\
&F_3(1,y) = 0, && F_4(1,y) = 1, \\
&F_5(1,y) = 1, && F_6(1,y) = 0, \\
&F_7(1,y) = 0.
\end{aligned} \tag{5.24}
$$

In order to make the superconductivity results from the localized defect, we choose F_6 to vanish, which obviously makes F_7 vanish like in the linear perturbations, since there is no electric field to develop the hair in the region infinitely far away from the symmetry axis. Moreover, these boundary conditions make the solutions reduce to AdS_4 away from the symmetry axis as well.

On the symmetry axis $x = 1$, we impose regularity in a sense that the metric functions and fields do not develop a kink like before

$$
\begin{aligned}
&\partial_x F_1(0,y) = 0, && \partial_x F_2(0,y) = 0, \\
&\partial_x F_3(0,y) = 0, && \partial_x F_4(0,y) = 0, \\
&F_5(0,y) = F_2(0,y), && \partial_x F_6(0,y) = 0, \\
&\partial_x F_7(0,y) = 0.
\end{aligned} \tag{5.25}
$$

Lastly, we impose regularity on the non-extremal horizon at $y = 0$ by imposing that temperature of the black hole horizon is uniform. We omitted to report these mixed boundary conditions, since they are rather lengthy expressions and unenlightening.

In order to use the Einstein-DeTurck trick, we need to provide a reference metric for the ansatz (5.20), as we mentioned in the section (4.4) before. Note that the AdS-Schwarzschild black hole (2.3) can easily provide that, since it has the same boundary conditions with the solution we are looking for and has a simple closed form expression.

We choose the metric (5.13) and the gauge field (5.14) combined with the zero mode we found in the previous section as our seed for the Newton-Raphson algorithm. Note that since zero mode perturbations are continuously connected to the solution we are looking for (that is there exists a parameter, the strength of the defect α, that we can use to label solutions), we had no issue regarding the issues related to the choice of seed. We observed that our solution converged with a quadratic error in each iteration for any amplitude if the grid was sufficiently large. Some of the convergence properties for this solution are given in the appendix A. Since the resulting solution would be the hairy version of the black mushroom solution (5.13), we will denote this solution as *hairy black mushroom* henceforth.

After solving the equations of motion, our result for the shape of the scalar hair for the profile $(1+r^2)^{-4}$ at temperature $T = 0.096$ is shown in figure (5.9). As one can see, the hair is formed outside of the black hole like in global holographic superconductors by the same mechanism of condensation we mentioned in the previous chapter. For comparison, look at the shape of the scalar hair for the global holographic superconductor (3.2) and observe it doesn't have a radial dependence. Additionally, we explicitly checked that this solution is indeed a nonlinear solution of the equations of motion by scaling our linear solution for Φ in the previous section and using that as a seed. In principle, this should still give the same solution and we observed that it did.

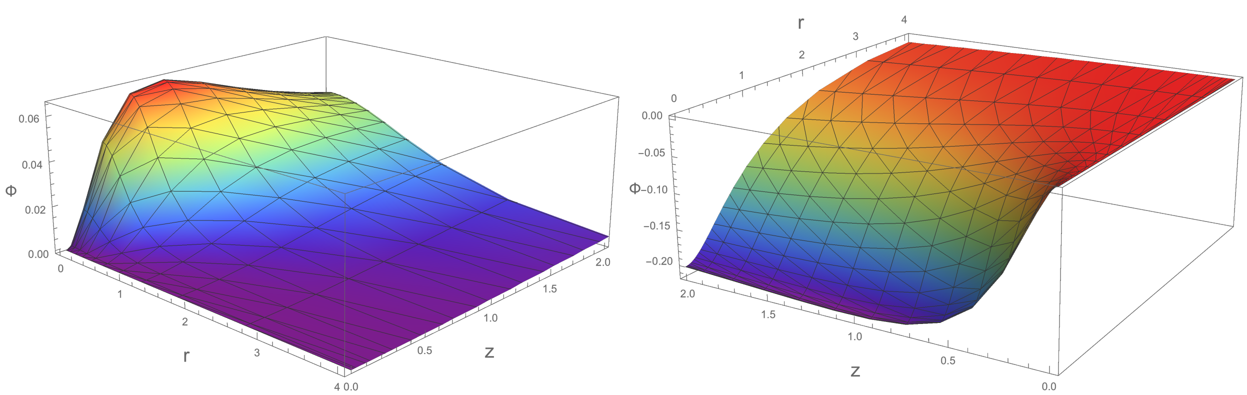

Figure 5.9: Back-reacted local scalar hair in AdS spacetime for $\alpha = 3$ (left) and $\alpha = 6$ (right). Observe the interesting behavior for small α around $z \approx 0.75$ which we also observed in the probe-limit.

As can be seen in figure (5.9), unlike the global holographic superconductors, the scalar hair is localized around the symmetry axis. The reason is the same as why zero modes appear around that region: The effective mass of the charged scalar field becomes the same as the actual mass of the scalar field farther away from the axis and the horizon getting weaker, therefore no condensation via violating BF bound and pair production occurs away from the region near the symmetry axis.

The radially dependent VEV of the scalar field $\langle\Phi(r)\rangle$, and the charge density $\rho(r)$ on the boundary for the same profile and temperature with $\alpha = 6$ is shown in figure (5.10). Again, we note that for the global holographic superconductors these quantities would be mere constants.

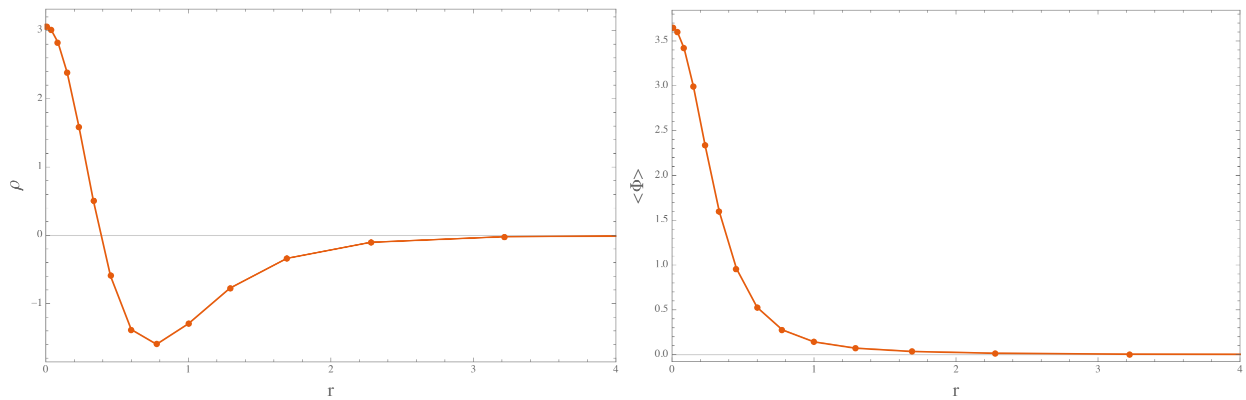

Figure 5.10: The charge density induces by the charged defect (left) and the vacuum expectation value of the scalar field (right) on the boundary for the hairy solution with the parameters mentioned in the text. As expected, superconductivity is localized around the origin and smoothly transforms to the normal phase as $r \to \infty$.

As one can inspect from figure (5.10), the expectation value of the charged scalar $\langle\Phi\rangle$ has a radial dependency and is most prominent around the charged defect, while vanishing smoothly as we move farther away from the origin $r = 0$. We saw that this is always the case for different defect profiles we investigated at different temperatures as well, along with the shape of the hair in (5.9). That means superconductivity is most robust around the charged defect and smoothly transforms to the normal phase as we go away from the origin of the boundary. Hence, we call this novel phenomenon *local holographic superconductivity.*

It is interesting to note that the VEV $\langle\Phi(r)\rangle$ doesn't follow the shape of the charge density, as one would naively expect, but rather modulated by the shape of the chemical potential. So this shows that there is a certain ring on the boundary where there is little-to-no charge but it is superconducting nonetheless, as well as it is energetically more expensive to go to the normal phase and then go back to the condensed phase on the boundary for strongly interacting field theories.

However, the most novel effect of the presence of a charged defect is shifting the place of the maximum amplitude of the scalar field for small α in AdS. As we can see from figure (5.9), the maximum of the scalar hair is not near the black hole horizon, but rather shifted away from it. Observe that as we increase the strength of the defect, this effect becomes less prominent. We relate this fact to the geodesic equation for the spacetime which we will explore more in the chapter below. So we postpone our discussion of this fact from a gravitational point of view for later.

Although, as we will see, the gravitational explanation of this phenomenon is elegant, the field theoretical meaning of this effect is not so clear. By AdS/CFT dictionary and the meaning of the holographic direction, this result implies that superconductivity impacts the frequencies in the mid-IR range for low enough α more than it impacts the frequencies in the deep IR range, in contrast to the global case. So if we imagine sending some signal on this frequency range in the boundary, we should see novel effects due to this modulation. These effects should be explored more by perturbing our solutions and looking at the correlation functions. For example, looking at the conductivity and the evolution of the superconducting gap might give interesting results for the perturbations in the mid-IR range frequencies.

The corresponding physical picture in the field theory of this phenomenon is most likely coming from the strongly interacting nature of the underlying field theory, but again, we should emphasize that understanding this effect from the field theory perspective would be challenging with our current methods. Our best bet to understand this phenomenon would be with gravitation, which we try to interpret in the next chapter under the umbrella of the physics of hovering black holes and using the geodesic equation.

5.4 The Critical Temperature

It would certainly be interesting to investigate the dependence of the critical temperature T_c, that is the temperature for which the superconducting phase forms for a fixed charge q, to the strength α and compare it with the global case. In this section, we will do that by choosing a fixed charge and draw a horizontal line in figure (5.5) and interpolating the strength of the defect when it crosses q_{min} curves at different temperature.[2] The resulting behavior for the defect profile $\zeta(r) = (1+r)^{-4}$ is shown in figure (5.11) for different charges of the scalar field.

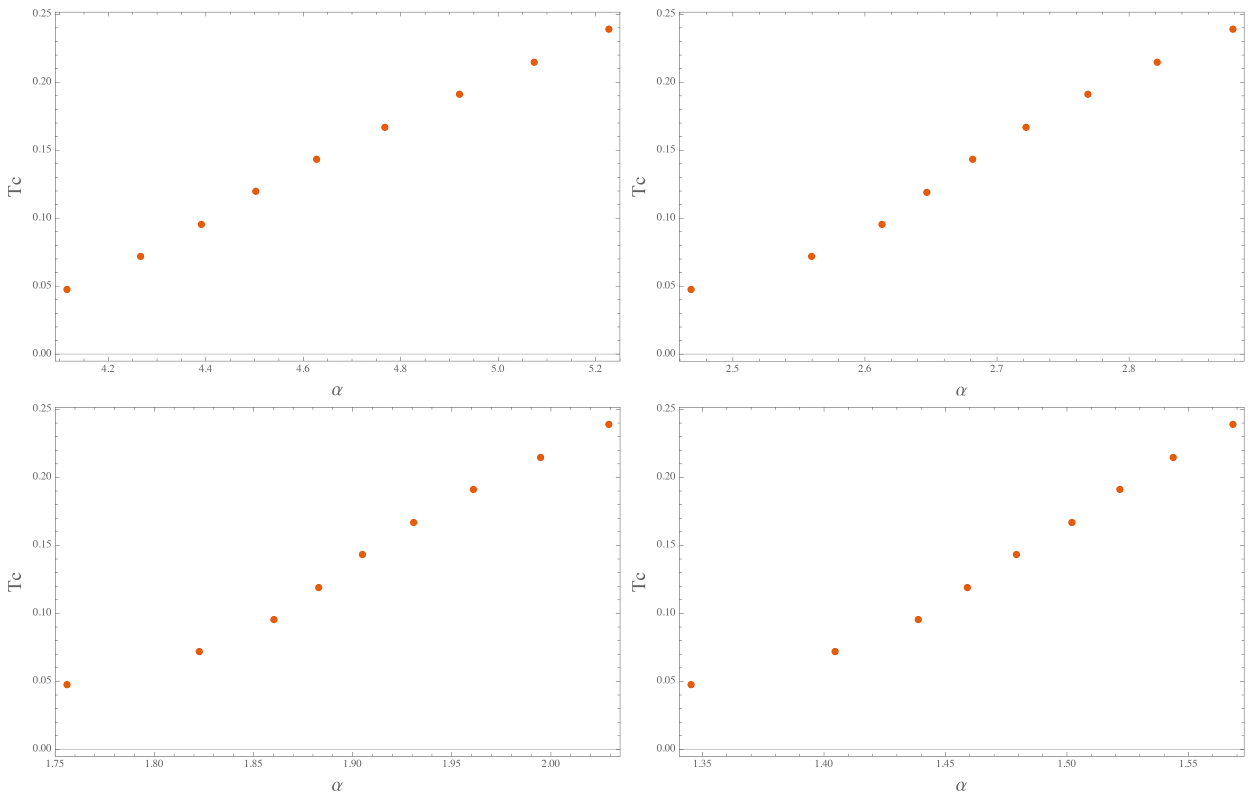

Figure 5.11: Dependence of the critical temperature T_c on the strength of the defect $\alpha = 3$ for the charges $q = 3$ (top-left), $q = 5$ (top-right), $q = 7$ (bottom-left), $q = 9$ (bottom-right).

As we can see the behavior is nonlinear for the charged defects, in contrast to the global case, where the critical temperature scales with the chemical potential linearly, $T_c \sim \mu$ in all regimes, by dimensional grounds. This is somewhat expected since the spherically symmetric charged defect is inherently nonlinear compared to the constant chemical potential in the global holographic superconductors. However, as we increase the strength of the defect α, it seems that the critical temperature begins to scale with the strength of the defect, which is consistent with the interpretation we had in section (5.2).

[2] We should note that there is an error associated with this interpolation. However, we are just looking for the proof of concept here, not the explicit numerical values. So in the end, we believe that this additional error shouldn't alter the behavior significantly.

It would be interesting to see that whether this effects are realized for real-world high-T_c superconductors, such as in cuprates. If this is the case, it might pave the road to modify the critical temperature to the desired temperature more precisely,[3] at the expense of sufficiently localizing the superconductivity in some region, rather than making it superconducting everywhere on the copper-oxide plane in cuprates. Still, if it isn't case, we believe that this work wouldn't be for naught though. We hope that if this type of behavior is not realized in experiments, it will still provide us with better understanding in which way the strange metal physics and the physics of AdS spacetime differs.

5.5 The Scaling Behavior and Free Energy

We also wanted to determine the scaling behavior of the scalar order parameter $\langle\Phi\rangle$ near the critical temperature T_c to check if there are any surprises. However, we found that the order parameter follows the usual second-order mean-field type behavior which is given by the scaling (3.2) as shown in figure (5.12) for the defect $\mu(r) = 3(1 + r^2)^{-4}$ near the critical temperature $T_c = 0.119$.

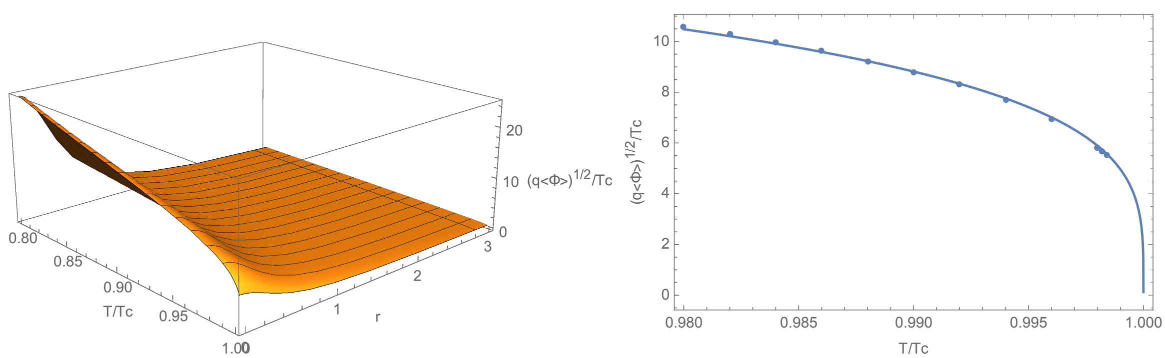

Figure 5.12: The scaling behavior of the order parameter near the critical temperature, for different radial distances (left) and specifically at the origin with a properly fitted curve given in the text (right). For the reason why we plot them this way, see [18].

We can see it is a mean-field type phase transition by the example fit we made for the scaling

[3] Even increase T_c for certain defects, which was our hope in the beginning of the study. However, we didn't find any evidence of it.

of $\langle\Phi\rangle$ at the origin. We find the best fit for these points to be $\frac{\sqrt{q_{min}\langle\Phi(0)\rangle}}{T_c} \approx 27.8774\left(1-\frac{T}{T_c}\right)^{1/4}$ when $T \approx T_c$, and from this we immediately see $\langle\Phi\rangle \sim (T_c - T)^{1/2}$, like in the global case [18]. The argument works in a similar fashion and plot would look similar for other cases, however possibly having different constants because of the different types of defects and strengths of them. Additionally, from figure (5.12) we see that if the superconductivity is more robust in some region, such as near the origin, the scaling behavior is sharper.

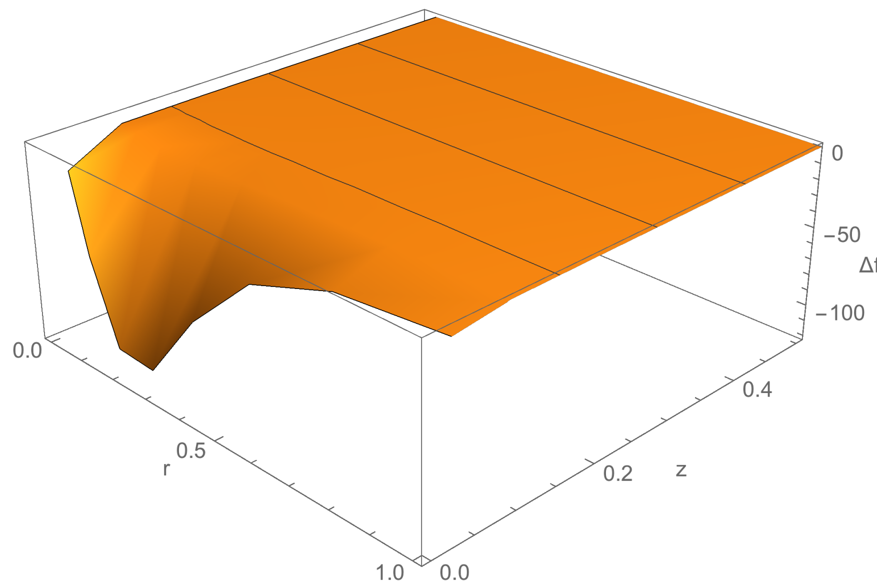

Figure 5.13: The difference between the free energy densities Δf of the hairy black mushroom and the black mushroom solutions for the profile $\mu(r) = 3(1+r^2)^{-4}$ at temperature $T = 0.096$. Note that $\Delta f \leq 0$ always.

Lastly, we decide to check the difference between the free energy of black mushroom and hairy black mushroom solutions, in order to confirm that the hairy black mushroom solution dominates over the black mushroom solution in the grand canonical ensemble. The difference between the free energy densities, Δf,[4] in AdS spacetime of these solutions are shown in figure (5.13) which is generated using the equation (2.15). Note that we haven't included Δf at the asymptotic boundary in our plots, since at this region Δf actually diverges. But as we noted before, these UV divergences

[4] Technically this is the grand potential, however we are going to us symbol f loosely as it is somewhat common in holography literature. Also we subtract the free energy density of hairless solution from the hairy solution

can be canceled with the addition of suitable counterterms like in the usual field theory, so they don't pose a threat to the argument we are making now.

Clearly, we see that $\Delta f \leq 0$ when $T < T_c$ everywhere on the spacetime, which implies that, after properly integrating by canceling the divergences due to the boundary to find the difference in the total free energy ΔF, the hairy black mushroom dominates below the critical temperature in the grand canonical ensemble, by the fact that $\Delta F \leq 0$ for the total free energy. In some sense, this is nothing surprising just by the point of view provided by the instabilities we mentioned before. Nonetheless, it was a reassuring check we made.

Chapter 6

Hovering Black Holes

In this chapter, we will briefly comment on the effects of the formation of a scalar hair at finite temperature to hovering black holes semi-quantitatively, which is discussed in [27] for the case without a scalar hair. Moreover, we will speculate about the bulk effects arising from disorder in the chemical potential at the boundary and discuss the possibility of hovering black holes with a planar horizon instead of a spherical one. As we will see, such black holes in AdS spacetime might result in extremely novel phenomenon and can have far reaching consequences for the field theory side.

6.1 Basics

For this we will follow the discussion in [24]. The motion of the particle with a mass m and charge q in spacetime is determined by the geodesic equation coupled to the electromagnetic field

$$\frac{dx^\nu}{d\lambda}\nabla_\nu\left(\frac{dx_\mu}{d\lambda}\right)=\frac{q}{m}F_{\mu\nu}\frac{dx^\nu}{d\lambda}. \tag{6.1}$$

Here, λ is an affine parameter and ∇ is the covariant derivative for the coordinate transformations. In our case, we consider a static and axisymmetric spacetime with a negative cosmological constant and want to learn if it is possible to put a black hole somewhere in the spacetime and get a stable solution. As the first approximation, we can consider our black holes small and extremal, namely, we can assume that they satisfy $|q| = m$ and treat them as charged point particles that obey the geodesic equation coupled to electromagnetism (6.1). So the problem reduces to finding the stationary points of this equation. Here by stationary points we mean that the worldlines of the particles for which particles have no acceleration in their rest frames. Expanding the equation (6.1) around the background (5.13), the (stable) stationary points can be found by minimizing the potential,

$$\mathcal{V} = \sqrt{-g_{tt}} - A_t. \tag{6.2}$$

We must make a couple of remarks before proceeding. First note that by the axisymmetry of our spacetime any extremum point should lie on the symmetry axis, namely $r = 0$. So, for a spherically symmetric charged defect we will only consider this axis and we will use the *thermal length* of the points on this axis defined by $l_T = \sqrt{-g_{tt}}$ to compare the potential $\mathcal{V}$ across different backgrounds.

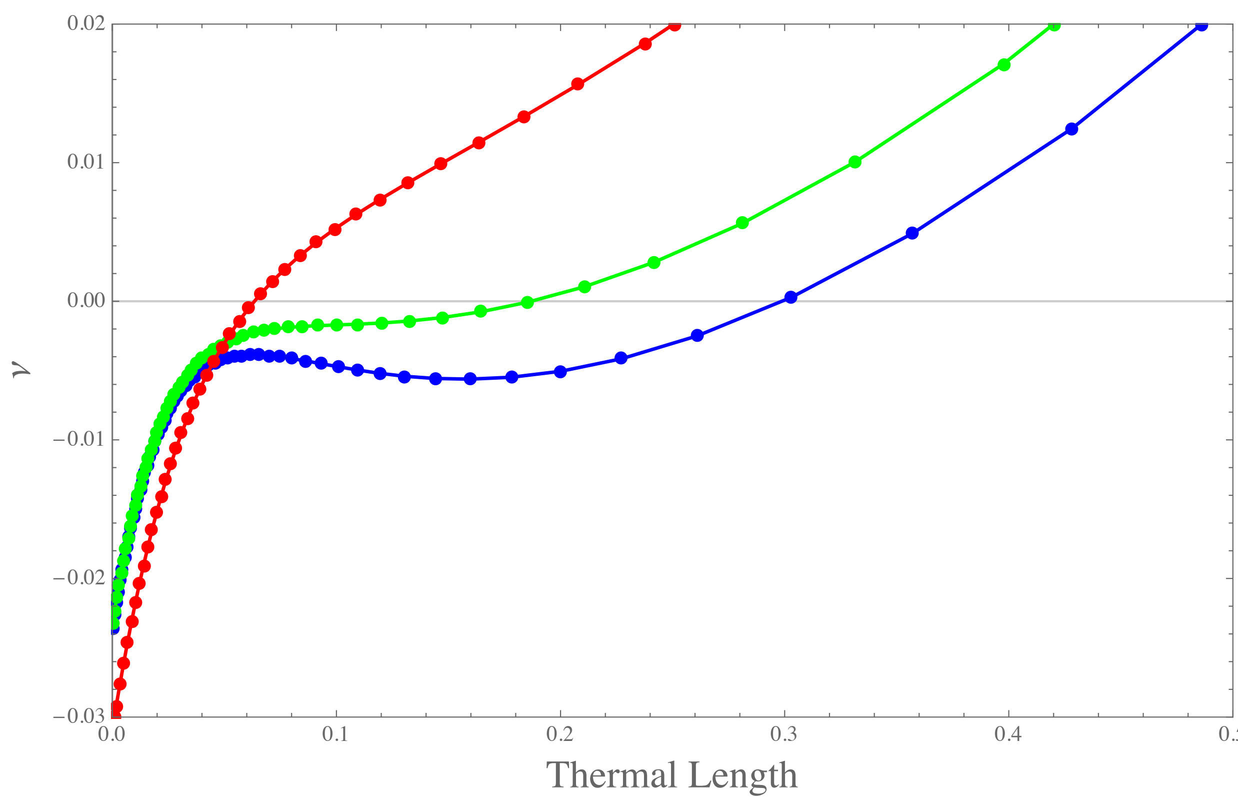

Figure 6.1: Plot of $\mathcal{V}$ without the scalar hair for the defect $\mu(r) = 7.1(1+r^2)^{-4}$ at the temperature $T = 0.014$ (blue), $T = 0.015$ (green), and $T = 0.024$ (red) on the symmetry axis $r = 0$. Note that there are two minimums in the blue curve, one at when the thermal length is zero corresponding to the black mushroom and one ot when the thermal length is around $\sqrt{-g_{tt}} \approx 0.175$, corresponding to a stable stationary point of the geodesic equation.

Moreover, observe that because of the normalization of the action (5.1), the potential $\mathcal{V}$ equals to 0 for the flat spacetime without electromagnetism for stationary points of the geodesic equation. This is an important choice, since we know particles with $\mathcal{V} > 0$ are not stable in flat spacetime, finding minimum of $\mathcal{V}$ is actually not sufficient and we must also look for the minimum below zero. A typical progression of the potential $\mathcal{V}$ with temperature is shown in figure (6.1).

After non-thermal minimums are found, like in the second minimum around $\sqrt{-g_{tt}} \approx 0.175$ in the figure (6.1) above, it is possible to "grow" a black hole by putting a particle there and slowly increasing its size, until a hovering black hole forms, using the fact that the point we put the particle at is a stable stationary point of the geodesic equation. Although this idea is simple, implementing it is a great technical challenge, see [24] for more details how to construct these solution. We won't comment on building such solutions but we hope that it is in principle possible (and necessary) to construct such solutions accordingly.

6.2 Hovering Black Holes with Hair

The shapes of the potential $\mathcal{V}$ for the cases with and without a hair at the temperature $T = 0.014$ for the charged defect $\mu(r) = 7.1(1 + r^2)^{-4}$ are given in figure (6.2). Inspect that for the hairy solution, the potential $\mathcal{V}$ is slightly lower than the one without a hair around the second minimum $\sqrt{-g_{tt}} \approx 0.175$. This is exactly what we would expect since we know that the black hole in deep IR is discharged slightly when the scalar hair is formed, which means that the hair formed outside of the black mushroom, as we described in the previous chapter. As a result of this, the scalar hair gravitationally attracts more towards to the second minimum. Observe that this effect is tiny, but not negligible in the numerical accuracy we are working in.

There are many interesting questions we might ask for these systems, from both the bulk and boundary point of views. Unfortunately, we should add a disclaimer and mention that answering many of these question will not be in our grasp without constructing the solution of hairy black hole which we have already noted is nearly impossible to construct with our current numerical techniques. However, we can get some idea regarding which answers would be more plausible using

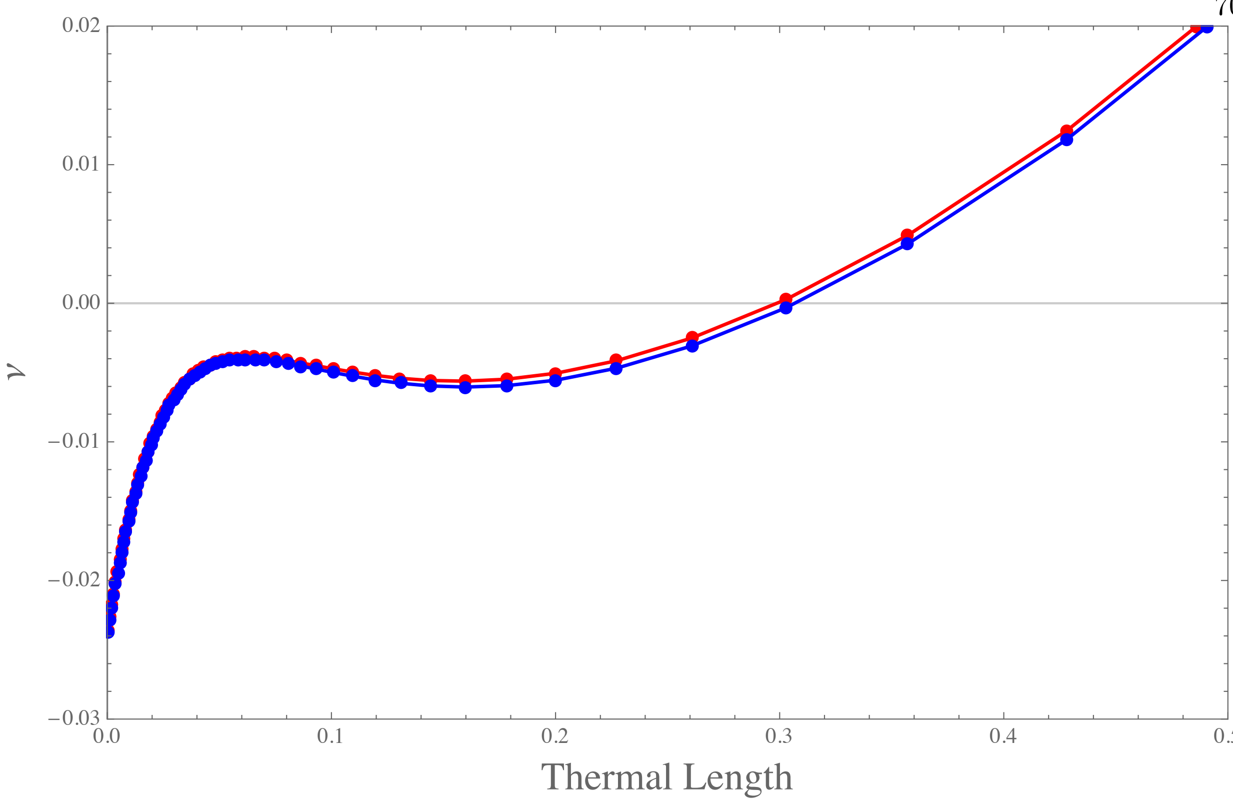

Figure 6.2: The potential $\mathcal{V}$ for the solutions with (blue) and without (red) hair, given on the symmetry axis $r = 0$. As one can see, they are nearly the same curve, except there is a slight decrease in the second minimum of the potential for the case with the scalar hair.

physical reasoning.

The first question we ought to ask is which of the two solutions, the hairy black mushroom we found in the previous chapter or the hairy black mushroom with hovering black hole as indicated by the potential $\mathcal{V}$, would be the dominant solution and in what regimes and ensembles? It is intuitive to expect that for a sufficiently dense scalar hair, it would eventually form a hovering black hole by collapsing onto itself. Overall, by figure (6.2) and the fact that the minimum slightly lowered, we see that forming hovering black hole must be easier in general, therefore this argument seems reasonable.

Also, this is rather evident from the shape of the hair in figure (5.9). As we can see and as noted in the previous chapter, the scalar field is localized in the mid-IR range near the symmetry axis, which roughly corresponds to the minimum of the potential $\mathcal{V}$ when α is small enough. This shape of the hair makes total sense then, since the geodesic equation creates a sort of potential well in AdS with the combination of AdS compression and electromagnetic push which makes the scalar field to move over to this region as a result. Although they are in the same spirit, we should note that the potential $\mathcal{V}$ and the potential that gives the equilibrium of forces in this argument are different in general. On the other hand, when α is large, the scalar hair becomes more spread out in the spacetime, which makes the shape in figure (5.9) to disappear.

The second question we might ask is whether the order of formation of a hair and hovering black hole makes any difference. Again, we can't say anything regarding issue with the results and tools we have and further studies are needed.

6.3 Planar Hovering Black Hole

So far, the horizon of the hovering black hole we mentioned was spherical. In passing, we will discuss the possibility of the existence of hovering black holes, with a *planar* horizon along with its novel implication for the field theory.

Before we begin our discussion, we should note that everything we will say below assumes the existence of such solutions, which we provide the evidence for. However, it is also likely that such solutions might not exist and even if they do, they might not be stable.[1] So, without constructing the solution, everything we say should be taken with a grain of salt and being cautious is the best bet. However, we include the discussion here, because we believe the possible effects are extremely novel and may indicate the end points of disordered instabilities and deserves a mention.

With these considerations in mind, start with imagining the case for which there are multiple defects added in a disordered fashion in the asymptotic boundary like in figure (6.3).[2] The potential $\mathcal{V}$ would definitely be altered, and it would be (possibly) altered in such a way that there would be multiple copies of the shape shown in figure (6.1) under each defect in the direction of z. Now consider the case for which these defects are either sufficiently close or sufficiently strong. Then it

[1] This instability argument can be made for the spherical black hole as well.
[2] Putting an array of them might also work, but here we will only consider the disordered case.

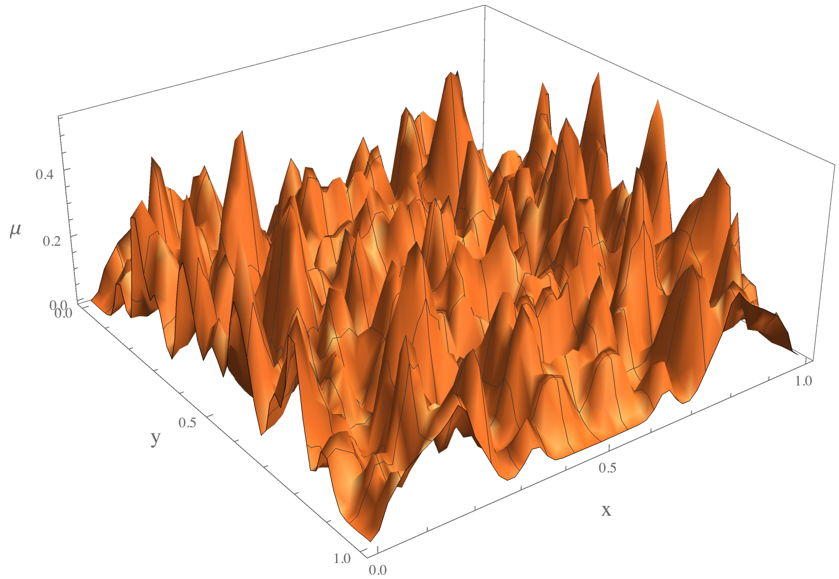

Figure 6.3: Typical profile of disordered chemical potential. Here Gaussian defects are used to construct a patch of this random chemical potential.

is not unreasonable to think that such minimums of potentials combine into a region so that the every point on the region is below zero.

Now in that region, instead of a single extremal particle like above, put an extremal and thin *slab*. Such a slab would be stable, like the small spherical black hole, because it lies in the region where potential is below zero. However this doesn't guarentee that the slab will be flat. It might be curved according to the actual shape of the region.

Now grow the slab incrementally. If we grow it sufficiently large, it will be a hovering black hole, but with a planar horizon topology. Again, we ignore the issues regarding instability, this planar solution might nucleate into a number of spherical hovering black holes, and be similar to the solution in [3], but with a back-reaction. But assume for a moment that there is a certain regime where it is stable and its horizon is planar and maybe more importantly connected. This case looks schematically like in the diagram (6.4) below.

Why do we want this hovering black hole with planar (or more importantly connected) topology? In order to answer that, consider the following thought experiment. Imagine that we perturb the field theory in the UV, for example by adding an external electron to the field theory.

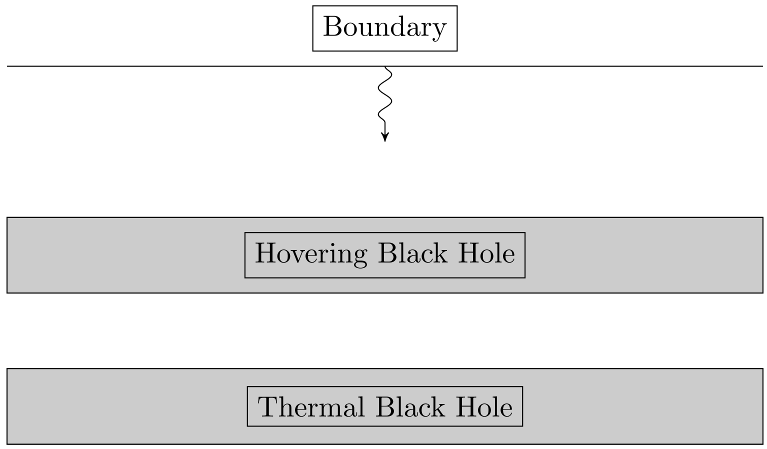

Figure 6.4: Diagrammatic representation of a planar hovering black hole. Here the curly line indicates the RG evolution of a perturbation in the field theory, such as adding an external particle.

By the AdS/CFT dictionary, the interaction of this electron with its surroundings would be dualized by the motion of the perturbation induced by this electron inside AdS spacetime, represented by the curly line in figure (6.4). Without the hovering black, this perturbation would move towards to the deep IR where a black hole corresponding to the thermal physics resides. Naturally, it will move into this black hole and won't come out. This is basically the AdS dual of coming into thermal equilibrium in the field theory, which is the expected behavior for such systems.

Now consider the case with the planar hovering black hole, i.e consider CFT with disordered chemical potential. In this case before this perturbation reaches to the deep IR, it should move into this newly appeared black hole first. But one good thing about black holes is that once something is inside, it never comes out, and this perturbation is no exception.[3] From the field theoretical point of view, this means that this external electron *cannot* reach into thermal equilibrium (or cannot diffuse), but *localizes* because of the disorder, like in the usual Anderson localization. We see the reason why having one-piece hovering black hole horizon is important now, because this argument would not work in the case where there is a hole in the black hole horizon. Although we should mention that, in that case, it will still make coming into thermal equilibrium harder, if not impossible, by weakening the signal when it crosses disconnected horizon.

[3] At least in the leading order. Hawking radiation will emit the perturbation to deep IR by quantum effects. But we are working in large-N, which will suppress these effects.

It is no coincidence that we use the term *localization* here, because we think this physics might be related to the localization using the heuristic reasoning that having a black hole in the mid-IR scale basically represent a huge number of states in that energy regime [36] and localization also holds states by not allowing them not to diffuse. This connection ought to be established more precisely since it might reveal the dual mechanism of localization in the strongly interacting systems.

Moreover, we can interpret the result of this thought experiment from the perspective of the information spread in strongly coupled CFTs at finite density under the presence of strong disorder. This result implies that the information from the high energy scales *does not* reach into the low-energy regime. The low-energy physics always seems irrespective of UV information which in some sense implies that the low-energy physics of such system should behave irregardless of any perturbation in UV. We can not find any related phenomenon to this effect in field theory.

Lastly, we can similarly look at the effects of disorder to the confinement of degrees of freedom in strongly coupled CFTs using Wilson loops. Recall that the Wilson loops are dualized by the string worldsheet in the AdS spacetime and deconfinement is indicated by the process of the top of worldsheets becoming disconnected due to the black hole horizon.

Like in the AdS-RN case we described in chapter (2), the string worldsheet would be disconnected because of the black hole horizon, but the black hole that rips it apart would be the hovering one, not the thermal one. Since the scale of the hovering black hole position in AdS is set by the scale of disorder, deconfinement happens at the scale of disorder, which is much earlier than the thermal scale in the energy scale. So this implies that disorder makes the theory deconfine at higher energy scales.[4]

This result might be somewhat argued from the fact that disorder makes it harder for the degrees of freedom to interact with each other, so they become deconfined earlier in the energy scale. We should note that this effect is most-likely due to the large-N limit in which we are

[4] Since we are considering irrelevant defects here, the dependence on the specific direction in the boundary shouldn't matter because they will die off as we go deep in AdS. However, the Wilson loop might have a nontrivial shape near the boundary.

working, but it would be a good exercise to investigate it if there is any corresponding phenomenon in QCD as well.

There are so many questions to be asked and beautiful physics is waiting to be found in these systems. However, extraordinary claims requires extraordinary evidence so we cannot be precise enough to see whether the claims above contains any truth without constructing such solutions. The worst part of constructing such solutions is that they are cohomogenity-1 instead of cohomogenity-2, so numerics become extremely challenging, bordering impossible. It might be useful to find some sort of toy model that contains similar physics like the one suggested above.

Chapter 7

Conclusion and Outlook

In this study, we constructed a gravitational dual for the local holographic superconductors: Superconductivity confined in a local region as a result of a spherically symmetry charged defects. We investigated its similarities and differences with each other and with the global case. We found that the critical temperature can be tuned at the expense of making superconductivity local. Also we concluded that its gravitational dual in AdS might contain a hovering black hole by investigating the stationary points of the geodesic equation.

We first studied the linear scalar instabilities in AdS spacetime under the presence of the charged defects and discovered that the zero modes are present in such spacetime. We observed that the perturbations are more robust in a region around and under the defect in the direction of z for sufficiently high charge or low temperature. We characterized the minimum charge and temperature needed for such instabilities to be present.

Secondly, we constructed the gravitationally back-reacted solution corresponding to the end points of these scalar instabilities. We found that a local scalar hair develops around the black hole as a result of violating BF-like bound. Interestingly, we find that superconductivity is most robust not in the deep IR, but between the IR and UV regimes of the theory if the defect is small enough in magnitude. We relate this observation to the geodesic equation in our hairy black mushroom solution. We briefly commented on what it would imply for the field theory, but this question remains open. Lastly, we saw that it was possible to change the critical temperature with defects nonlinearly and commented on the scaling behavior and free energy of the solution we constructed.

In order to understand local holographic superconductivity phenomenon and its relation to the normal phase of charged defects better, it is imperative that we understand the correlators of the currents and the stress-energy tensors, both in the normal and superconducting phases. Especially studying conductivity would help us detect the differences between the charged defect and the uniform chemical potential more precisely, and would allow us to see how superconducting gap evolves. Because of the nontrivial effects we have seen in the mid-IR regime (such as the possibility of having a hovering black hole or having the scalar hair maximized in amplitude in the mid-IR scales for small defects), there might be nontrivial effects of the defect in the mid-range frequencies for the conductivity. We attempted to implement this in the spirit of [26], but hit the usual problem of gauge fixing for perturbing numerical black holes. We leave this for our future work.

Also, we discovered that having a hair in the spacetime lowers the non-thermal minimum of the potential for the stationary point of the geodesic equation by attracting more matter through there and in principle making it easier to form a hovering black hole. We think that the interactions between the hovering black holes and the scalar hair need further study to understand which solutions dominate in which ensemble to give us a complete picture of the phase space, and find a region and ensemble for which the local holographic superconductivity we solved for dominates. For example, it would be interesting to form a scalar hair and then hovering black hole and in reverse order to compare the resulting solutions to look for any differences. But again, these solutions pose great technical challenges.

Lastly, one interesting direction for the future research for CFTS with non-uniform chemical potential might be applying charged defects randomly and constructing the full solution for disordered chemical potential, which we discussed their physics without constructing the solution. We argued that for such solutions with sufficiently disordered and/or strong defects there might exists a region in AdS at fixed z for which the potential is below zero and contains a minimum. Using that possibility, we argued that the possibility of growing a hovering black hole, like in [24], but instead of having a spherical black hole hovering, we argued that it might have a planar black hole hovering above the deep IR.

We think planar hovering black holes would be extremely interesting consequences for the boundary field theory. Since the deep IR and the UV regimes of the theory are separated **completely** by a black hole, we believe that dissipation-like effects might occur in the mid-IR scale of the theory, determined by the scales of disorder, rather than thermal scales, and information from high energy degrees of freedom cannot evolve to low energies. We argued that such physics might be related to the localization in the context of strongly coupled conformal field theories, noting that similar effects happen in localization under disorder and black holes basically represent huge number of states by AdS/CFT dictionary, and might be the related to the physics in [3], as well as shed more light on the mid-IR effects of the hairy black mushroom solutions. Also we argued that it might have consequences for deconfinement under the random potential by making deconfinement scale much earlier than the thermal scale.

However, we should repeat that these solutions would be cohomogenitiy-1, which makes them extremely challenging to solve numerically. We experienced that even getting the analytical equations is computationally very expensive. Again, a simple toy model containing the same physics would be very handy in this situation and would provide us a way to understand the nature of these extraordinary effects better.

Lastly, we think there is a high possibility that similar effects discovered in local holographic superconductors might be observed in real-world high-T_c superconductors if they are formed around a local doped region.[1] We challenge experimentalists to realize the similar system in cuprates or any other high-T_c superconductors to see if the modification of the critical temperature is possible in a similar fashion. We hope this will not only provide a novel way to modify the critical temperature, but will be a useful test for AdS/CMT research program and how similar these systems are.

[1] This is motivated by the observed match between cuprates and holographic lattices, see [26].

Bibliography

[1] Martin Ammon and Johanna Erdmenger. Gauge/gravity duality: foundations and applications. Cambridge University Press, 2015.

[2] Tomas Andrade. Holographic lattices and numerical techniques. arXiv preprint arXiv:1712.00548, 2017.

[3] Dionysios Anninos, Tarek Anous, Frederik Denef, and Lucas Peeters. Holographic vitrification. Journal of High Energy Physics, 2015(4):27, 2015.

[4] Neven Barišić, Mun K Chan, Yuan Li, Guichuan Yu, Xudong Zhao, Martin Dressel, Ana Smontara, and Martin Greven. Universal sheet resistance and revised phase diagram of the cuprate high-temperature superconductors. Proceedings of the National Academy of Sciences, 110(30):12235–12240, 2013.

[5] Mike Blake, Aristomenis Donos, and David Tong. Holographic charge oscillations. Journal of High Energy Physics, 2015(4):19, 2015.

[6] Peter Breitenlohner and Daniel Z Freedman. Positive energy in anti-de sitter backgrounds and gauged extended supergravity. Physics Letters B, 115(3):197–201, 1982.

[7] Peter Breitenlohner and Daniel Z Freedman. Stability in gauged extended supergravity. Annals of Physics, 144(2):249–281, 1982.

[8] Jiunn-Wei Chen, Ying-Jer Kao, Debaprasad Maity, Wen-Yu Wen, and Chen-Pin Yeh. Towards a holographic model of d-wave superconductors. Physical Review D, 81(10):106008, 2010.

[9] Toby Crisford, Gary T Horowitz, and Jorge E Santos. Testing the weak gravity-cosmic censorship connection. Physical Review D, 97(6):066005, 2018.

[10] João Pedro Alves da Silva. Ads black holes from localized boundary sources. 2015.

[11] O. DeWolfe. TASI Lectures on Applications of Gauge/Gravity Duality. ArXiv e-prints, February 2018.

[12] Oscar JC Dias, Jorge E Santos, and Benson Way. Numerical methods for finding stationary gravitational solutions. Classical and Quantum Gravity, 33(13):133001, 2016.

[13] Bernhard Edegger, Vangal N Muthukumar, and Claudius Gros. Gutzwiller–rvb theory of high-temperature superconductivity: Results from renormalized mean-field theory and variational monte carlo calculations. Advances in Physics, 56(6):927–1033, 2007.

[14] Thomas Faulkner, Hong Liu, John McGreevy, and David Vegh. Emergent quantum criticality, fermi surfaces, and ads 2. Physical Review D, 83(12):125002, 2011.

[15] Dimitrios Galanakis, Ehsan Khatami, Karlis Mikelsons, Alexandru Macridin, Juana M.a García Moreno, Dana A. Browne, and Mark Jarrell. Quantum criticality and incipient phase separation in the thermodynamic properties of the hubbard model. Philosophical transactions. Series A, Mathematical, physical, and engineering sciences, 369 1941:1670–86, 2011.

[16] Steven S Gubser. Breaking an abelian gauge symmetry near a black hole horizon. Physical Review D, 78(6):065034, 2008.

[17] Steven S Gubser, Igor R Klebanov, and Alexander M Polyakov. Gauge theory correlators from non-critical string theory. Physics Letters B, 428(1-2):105–114, 1998.

[18] Sean A Hartnoll, Christopher P Herzog, and Gary T Horowitz. Building a holographic superconductor. Physical Review Letters, 101(3):031601, 2008.

[19] Sean A Hartnoll, Christopher P Herzog, and Gary T Horowitz. Holographic superconductors. Journal of High Energy Physics, 2008(12):015, 2008.

[20] Sean A Hartnoll, Andrew Lucas, and Subir Sachdev. Holographic quantum matter. arXiv preprint arXiv:1612.07324, 2016.

[21] Matthew Headrick, Sam Kitchen, and Toby Wiseman. A new approach to static numerical relativity and its application to kaluza–klein black holes. Classical and Quantum Gravity, 27(3):035002, 2010.

[22] Gerard't Hooft. Large n. In Phenomenology Of Large Nc Qcd, pages 3–18. World Scientific, 2002.

[23] Gary T Horowitz. Introduction to holographic superconductors. In From gravity to thermal gauge theories: the AdS/CFT correspondence, pages 313–347. Springer, 2011.

[24] Gary T Horowitz, Nabil Iqbal, Jorge E Santos, and Benson Way. Hovering black holes from charged defects. Classical and Quantum Gravity, 32(10):105001, 2015.

[25] Gary T Horowitz, Jorge E Santos, and Chiara Toldo. Deforming black holes in ads. arXiv preprint arXiv:1809.04081, 2018.

[26] Gary T Horowitz, Jorge E Santos, and David Tong. Optical conductivity with holographic lattices. Journal of High Energy Physics, 2012(7):168, 2012.

[27] Gary T Horowitz, Jorge E Santos, and Benson Way. Evidence for an electrifying violation of cosmic censorship. Classical and Quantum Gravity, 33(19):195007, 2016.

[28] Martin Klanjšek. A critical test of quantum criticality. Physics, 7:74, 2014.

[29] Juan Maldacena. The large-n limit of superconformal field theories and supergravity. International journal of theoretical physics, 38(4):1113–1133, 1999.

[30] Horatiu Nastase. String Theory Methods for Condensed Matter Physics. Cambridge University Press, 2017.

[31] MR Norman and C Pepin. The electronic nature of high temperature cuprate superconductors. Reports on Progress in Physics, 66(10):1547, 2003.

[32] Joseph Polchinski. String theory: Volume 2, superstring theory and beyond. Cambridge university press, 1998.

[33] Lloyd N Trefethen. Spectral methods in MATLAB, volume 10. Siam, 2000.

[34] David Vegh. Holography without translational symmetry. arXiv preprint arXiv:1301.0537, 2013.

[35] Edward Witten. Anti de sitter space and holography. arXiv preprint hep-th/9802150, 1998.

[36] Jan Zaanen, Yan Liu, Ya-Wen Sun, and Koenraad Schalm. Holographic duality in condensed matter physics. Cambridge University Press, 2015.

[37] Hua Bi Zeng and Hai-Qing Zhang. Zeroth order phase transition in a holographic superconductor with single impurity. Nuclear Physics B, 897:276–288, 2015.

Appendix A

Convergence Tests

In this appendix, we discuss the convergence of our solutions briefly. By the pseudo-spectral collocation on Chebyshev grid, we know that the convergence can be improved exponentially by increasing the number of grid points. In order to explicitly check that, we chose the DeTruck norm $\mathrm{Max}(|\xi|^2)$ from the section (4.4) as our parameter indicating convergence and measured how it changes with increasing number of N for an $N \times N$ Chebyshev grid. For black mushroom and hairy black mushroom solutions, the results are shown in the figure below.

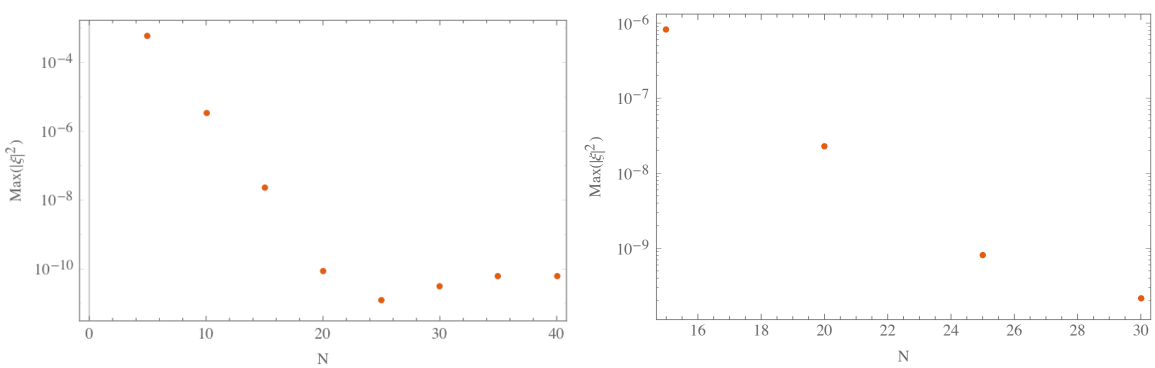

Figure A.1: Convergence tests for the black mushroom solution for $T = 0.239$ and $\alpha = 3$ (right) and for a hairy black mushroom solution for $T = 0.096$ and $\alpha = 3$ (left) for the profile $\zeta(r) = (1+r^2)^{-4}$.

As we can see, the convergence is improved exponentially with increasing the number of grid points until a certain point in which it becomes flat. We will generally assume that the convergence is reached when the error of the solution is below $10^{-6} - 10^{-7}$ for both for the DeTurck norm and the errors in the NR algorithm (this is reasonable since we are working with 8 significant figures). Therefore it was generally sufficient to use 20×20 to 30×30 grids for our solutions. However, we sometimes needed to calculate quantities in 70×70 grid to reach the desired accuracy.

We should note that as the strength of the defect increases or the temperature becomes small, the convergence is decreased. In such cases, it is better and safer to use bigger grids. So in the cases where we observed the maximum value of DeTurck norm increases, we increased the grid number proportionally to reach the desired accuracy. However, we discovered that in the end it didn't matter too much, since for the majority of the quantities we are looking for, such as scalings, hasn't been affected by the errors we propagated and our results stayed robust. So when suitable, we opted to use a smaller grid to save time and computational resources.